Describing the Catalytic Role of Alkaline Earth Metals on the Thermal Activation of Cellulose

A DISSERTATION

SUBMITTED TO THE FACULTY OF

UNIVERSITY OF MINNESOTA

BY

Gregory Facas

IN PARTIAL FULFILLMENT OF THE REQUIREMENTS

FOR THE DEGREE OF

DOCTOR OF PHILOSOPHY

Adviser: Paul J. Dauenhauer

May 2020

Acknowledgments

Most importantly, I would like to thank my family, especially my parents George and Maria, and my brother Nick. I would not be here without your tremendous love and support, not just during my graduate studies but throughout my whole life. Your unwavering support and encouragement has always motivated me to achieve this dream of mine, even during the hardest of times. Without you, none of this would have ever been possible.

I'd like to recognize my thesis adviser, Paul Dauenhauer, for accepting me into his laboratory and giving me the opportunity to work on this exciting project and work with so many great people in this laboratory for the past few years. His guidance and mentorship has helped me develop tremendously over the past few years and for that I cannot thank him enough. Paul's approach to solving complex research problems with such creative and out-of-the-box ideas is something quite unique and commendable, and is something I hope to emulate with any scientific challenges I encounter going forward.

There are many members in my research group that have played a large role helping me along the way. In particular, I want to thank Vineet Maliekkal. Collaborating with you the past few years has been an amazing experience. Without your dedication and brilliant work, this project would not have been successful and this thesis may never have been written. You gave me great insight from a different perspective on how to think of pyrolysis chemistry and that pushed me to understand this system better than I ever could have. I also want to thank my mentors Dr. Christoph Krumm, Dr. Cheng Zhu, and Dr. Saurabh Maduskar for their help and initially teaching me about cellulose pyrolysis chemistry.

Additionally, I want to acknowledge the current and former colleagues in my research group: Gaurav Kumar, Choongsze Lee, Yutong Pang, Ankita Naik, Nathan Sidhu, Isaac Mastalski, Yuxiao Wu, Costas Papageorgiou, Dr. Alexander Ardaugh, Dr. Ali Zolghadr, Dr. Manish Shetty, Dr. Deepak Ojha Dr. Kristeen Joseph, Dr. Anagyros Chatzidimitriou, Dr. Katherine Vinter, Dr. Omar Abdelrahman, Dr. Charles Spanjers and Dr. Dae Sung Park. All of these people made coming into the lab an enjoyable experience every day and I want to thank you all for that.

Lastly, I want to thank the Chemical Engineering and Materials Science department here at the University for accepting me into to the program and allowing me to purse my graduate studies here. The people I have met through the department has given me another family away from home. This has been an experience I will always cherish and never forget.

Dedication

This thesis is dedicated to my family, especially to the ones who weren't able to experience this journey with me.

Abstract

Biomass fast pyrolysis has considerable potential for the production of renewable fuels and chemicals. Despite pyrolysis being studied for more than a hundred years, only a few commercial pyrolysis processes exist as the optimal feedstock composition and reaction conditions for this process remain unknown. The lack of process optimization can be attributed to the multiscale complexity of the process. During pyrolysis the constituents of biomass are fragmented in a matter of seconds through thousands of chemical reactions, that occur in multiple phases, and are simultaneously competing with various heat and mass transfer processes. All of these fundamental phenomena are understood poorly within pyrolysis literature. Pyrolysis is further complicated by alkali and alkaline earth metals that are naturally present in lignocellulosic biomass. These metals are known to alter pyrolysis chemistry and catalyze the initial breakdown of the polymer constituents of biomass. The main objective of this thesis was to investigate the mechanistic role of alkaline earth metals on the initial fragmentation of cellulose, the main component of biomass.

Fundamental knowledge into pyrolysis chemistry has been limited previously due to an inability to obtain intrinsic kinetic, a critical tool used to validate reaction mechanisms. The requirements for proper measurement of high temperature (>400 °C) biomass pyrolysis kinetics are presented. Most importantly, these requirements mandate that for proper measurement of kinetic data, experimental techniques must heat and cool reaction samples sufficiently fast to elucidate the evolution of reaction products with time, while also eliminating substantial reaction during the heating and cooling phases. The ability of the PHASR (Pulse Heated Analysis of Solid Reactions) micro-reactor technique and other

common pyrolysis reactor techniques to satisfy these requirements was discussed. PHASR can thoroughly satisfy all the requirements for measuring pyrolysis kinetics unlike other conventional reactor techniques.

The PHASR technique was then utilized to study the kinetics of calcium assisted activation of cellulose. Conversion of calcium doped films of α-cyclodextrin, a known cellulose surrogate, was measured over a range of reaction temperatures (370-430 °C) and calcium concentrations (0.1-0.5 mmol Ca^{2+}/g CD). The rate of conversion of α-cyclodextrin was significantly accelerated by the presence of calcium. Activation was shown to have a second order rate dependence on calcium concentration, suggesting the involvement of two calcium ions in the mechanism. First principle density functional theory calculations were performed on calcium catalyzed glycosidic bond cleavage and depict calcium as having two catalytic roles of disrupting hydrogen bonding in the cellulose matrix and stabilizing the transition state. The energetics from experiment and computations agree closely representing the first atomistic mechanism of metal catalyzed activation utilizing both experiments and computations.

Kinetics of magnesium assisted activation were then measured with PHASR experiments to discern any effects from the size of the catalytic ion on activation chemistry. PHASR experiments were performed in identical temperature and metal concentrations to the calcium experiments. Magnesium assisted activation exhibited identical behavior to the calcium case with energetics of activation matching within experimental error.

Tables of Contents

List of Tables viii

List of Figures ix

Chapter 1: Introduction 1

Chapter 2: Thesis Scope and Objectives 4

Chapter 3: Pulse Heated Analysis of Solid Reactions (PHASR) 10

3.1: Introduction 10

3.2: PHASR Design 12

3.3: PHASR Evaluation for Measuring Pyrolysis Reaction Kinetics 14

3.3.1: Small Biomass Length Scale 14

3.3.2: Temperature Measurement and Thermal Control 16

3.3.3: Temperature Ramp during Heating 18

3.3.4: Online Detection and Temperature Ramp during Cooling 22

3.3.5: Sweep Gas Flow Rate 30

Chapter 4: Calcium Assisted Activation of Cellulose 32

4.1: Introduction 32

4.2: α-Cyclodextrin as a Kinetic Surrogate for Cellulose 36

4.3: Experimental and Computational Methods 38

4.3.1: Preparation of Calcium Doped α-Cyclodextrin Thin Film Samples 38

4.3.2: PHASR Experiments 38

4.3.3: Quantification of α-Cyclodextrin Conversion 39

4.3.4: Computational Methods....39
4.4: Kinetics of Calcium Catalyzed Activation....41
4.5: Investigating the Role of the Anion on Activation....48
4.6: The Nature of Active Sites and Interpretation of Kinetic Data....54
4.7: DFT Calculated Energetics for Calcium Catalytic Cycle....59
4.8: Conclusions....63
Chapter 5: Magnesium Assisted Activation of Cellulose....64
5.1: Introduction....64
5.2: Kinetics of Magnesium Catalyzed Activation....66
Chapter 6: Conclusions....73
Bibliography....75

List of Tables

Table 3-1 Pyrolysis Reactor Performance and Thermal Limitations.....21

Table 3-2 Experimental Conditions and Reaction Parameters used to Calculate Operating Points.....27

Table 3-3 Characteristics of High Temperature Biomass Pyrolysis Reactors.....31

List of Figures

Figure 3-1 PHASR Reactor Design and Method 13

Figure 3-2 Pyrolysis Transport Map 15

Figure 3-3 Kinetics of Cellulose Initiation 19

Figure 3-4 Required Heating Rate for Biomass Sample Pyrolysis 20

Figure 3-5 Disparity in the Time Scales between Polymer Reactions and Conventional Analytical Techniques 23

Figure 3-6 Design Requirements for a Reactor-Detector Coupled System 25

Figure 3-7 Cooling Rate Requirement of Kinetic Biomass Pyrolysis Reactor 29

Figure 4-1 Kinetics of α-Cyclodextrin Conversion in the Presence of a Calcium Catalyst 42

Figure 4-2 Comparison of First Order Rate Parameters Measured at 415 °C to Integer Powers of Calcium Concentration 43

Figure 4-3 Comparison of First Order Rate Parameters to the Square of Calcium Concentration 43

Figure 4-4 Calcium Catalyzed Activation Rate Constants Plotted in Arrhenius Form 45

Figure 4-5 Global Interpretation of Calcium-Catalyzed Cellulose Activation 47

Figure 4-6 Time Resolved Conversion of α-Cyclodextrin with $Ca(NO_3)$ and $CaCl_2$ Salts at Three Different Conditions 49

Figure 4-7 Online Mass Spectrometer Monitoring of HNO_3 and HCl Evolution of Calcium Doped Cellulose Samples 52

Figure 4-8 Molecular Structures of Neat and Calcium Incorporated Cellulose 56

Figure 4-9 Reaction Energy Profile for Ca-Catalyzed Reaction in the Single Calcium Ion Case. 60
Figure 4-10 Reaction Energy Profile for Ca-Catalyzed Reaction with Two Calcium Ions 61
Figure 4-11 Optimized Transition State Structures 62
Figure 5-1 Kinetics of α-Cyclodextrin Conversion with Magnesium Catalyst 67
Figure 5-2 Comparison of First Order Rate Parameters to the Square of Magnesium Concentration 68
Figure 5-3 Magnesium Catalyzed Rate Constants Plotted in Arrhenius Form 69
Figure 5-4 Comparison of Total Apparent Rate Constants for Activation in the Presence of Magnesium or Calcium 71

Chapter 1: Introduction

Rapid increases in the global population and the industrialization of non-developed nations have led to surging demands for energy. Worldwide energy usage is predicted to increase by about 50 % or 250 quadrillion British thermal units by the year 2050.[1] Meeting this demand, combined with efforts to combat global climate change has promoted development of renewable and sustainable energy technologies. Lignocellulosic or nonedible biomass has received considerable attention as a potential renewable feedstock to help meet this demand.[2] The main appeal of lignocellulosic biomass is that it is a cheap carbon based feedstock (~ \$0.1 /lb_m carbon) that can directly produce liquid transportation fuel without drawing from traditional food sources.[3,4] Global interest and development in lignocellulosic biomass technologies is apparent with international governments such as the European Union proposing strategies where 25% of all transportation fuels are produced from biomass by the year 2030.[5]

Biomass can be converted into fuels or chemicals through thermochemical processes such as pyrolysis or gasification, or through fermentation and enzymatic biological routes.[6–8] Fast pyrolysis of lignocellulosic biomass is of considerable interest towards the production of liquid fuels. During pyrolysis, solid biomass is heated between 400 to 600 °C in inert atmosphere and the constituents of biomass undergo rapid thermal decomposition to produce a wide array of organic volatile compounds, permanent gases and solid charcoal.[9–11] Once the organic volatile compounds are condensed, they form bio-

oil which can then undergo catalytic hydrotreatment to produce liquid fuel or other chemicals.[12–14]

While pyrolysis has considerable appeal to directly produce renewable liquid fuels through a relatively low capital intensive process, there are currently only a few commercial pyrolysis processes. However, there is a considerable amount of engineering and optimization of pyrolysis processes that can be developed to improve the commercial appeal of this technology. In particular, the ideal process conditions (e.g. reactor type/ configuration, reaction temperature and pressure, etc.) to maximize the overall yield and stability of bio-oil have still yet to be determined, demonstrating the vast amount of engineering that can still be achieved. One major limitation towards complete process optimization for pyrolysis is a limited understanding of the fundamental processes occurring while deconstructing biomass.[15,16] During pyrolysis there are a significant amount of competing physical and chemical processes transpiring; various heat and mass transfer processes occur along with thousands of simultaneous chemical reactions that are occurring within all three phases of solid, liquid and gas.[17–19] Each of these fundamental processes has a significant effect of the final quality and yield of bio-oil but current process models are unable to account and understand how all of these fundamental processes affect the final product state.

An additionally complexity is the variable composition of different lignocellulosic feedstocks. Lignocellulosic materials are generally composed of three strongly connected biopolymers; cellulose, hemicellulose and lignin. The structure and amount of these biopolymers varies with each feedstock.[20,21] For example, softwoods are typically

composed of greater amounts of lignin than hardwoods and softwood lignin is mainly composed of only coniferyl alcohol units, while hardwood lignin contains a mix of coniferyl alcohol and sinapyl alcohol units.[22,23] Similarly, the chemical structure and composition of hemicelluloses can vary significantly between different feedstocks.[20] It is then evident that the chemistry and other fundamental processes during pyrolysis will be different for each feedstock due to the varying composition and chemical functionality within each biopolymer. Lignocellulosic feedstocks also contain significant amounts of inorganic elements such as; silicon, alkali and alkaline earth metals (e.g. calcium or potassium), and transition metals like iron or copper. These metals have a significant effect on pyrolysis chemistry, and are generally viewed to reduce the yield of bio-oil while increasing the amount of char formed during pyrolysis.[24,25] Unfortunately, current process models do not sufficiently incorporate how the starting feedstock composition influences the chemistry and final result of pyrolysis.

Moving forward, it is pertinent that pyrolysis models accurately describe these fundamental processes and incorporate how the starting feedstock composition influences these processes and the final process yields. To expand these models, new experimental and computational approaches are required. These approaches must be able to carefully examine each of these aspects without having experiments and results be convoluted by the other various factors and phenomena occurring during pyrolysis.

Chapter 2: Thesis Scope and Objectives

Biomass pyrolysis has been a heavily studied process with publications dating back to as early as the 1850's.[26] Despite extensive studies into the fundamental chemistry of biomass pyrolysis there is no complete model to describe the full chemical reaction network. Studies looking to provide insight into the fundamental chemistry frequently focus on the cellulose component of lignocellulosic biomass.[26–28] Cellulose is a long straight polymer of glucose monomers connected by β-1-4 glycosidic linkages. Cellulose is mainly studied since it is the most abundant component of lignocellulosic materials (40-60 wt. %), and is chemically and structural consistent among all lignocellulosic materials, unlike the hemicellulose and lignin fractions of biomass.[20,21] Thus, using cellulose as the starting reactant allows for probing the majority of the chemistry during biomass pyrolysis. The results from experiments pyrolyzing cellulose can then be applied to reaction network models for individual feedstocks and then the effects from the other components on the reaction chemistry can be accounted for in a more facile manner.

Over the last forty years, numerous studies have helped develop a general reaction sequence for how cellulose pyrolysis chemistry proceeds. Once cellulose is rapidly heated to typical reaction temperatures, the polymer chains breakdown to form a short lived (<100 milliseconds) intermediate liquid phase that is a mixture of depolymerized cellulose, and dissolved gases (CO, CO_2).[17,29–31] From this intermediate liquid, char, permanent gases (CO, H_2, CO_2 etc.), and organic volatile compounds are formed. The organic volatile compounds, sometimes referred to as tars, are general group into product classes such as

anhydrosugars, furans, pyrans and light oxygenates. After formation, these organic volatile compounds can further react to produce additional amounts of char, light oxygenates and permanent gases. Conventionally, the formation of the intermediate liquid and the initial formation of products from this liquid are classified as primary reactions. Any subsequent reactions of the primary products are classified as secondary reactions.

While many publications have detailed possible reaction pathways in cellulose pyrolysis, reaction models are still missing key pieces of information. In particular, the chemical mechanisms of important reaction steps; such as the initial fragmentation of the starting polymer chain or the formation of the main products such as levoglucosan and furans are not completely detailed, leading to numerous and conflicting reaction models.[16,32–35] Complete mechanistic models have not been developed due to conventional experimental techniques inability to collect chemical kinetic data during typical process conditions. Insufficient kinetic data is problematic as kinetics are frequently used to support chemical mechanisms by constructing reaction rate expressions (i.e., reaction rate orders), comparing measured apparent activation energies with the energetics from computationally proposed mechanisms, and providing mechanistic explanations determined from kinetic isotope effect experiments.[36–39]

Currently, most studies utilize techniques such as thermogravimetric analyzers, single-shot drop furnaces, flash bulb pyrolyzers, and resistively heated surface pyrolyzers.[15,40–44] With each of these systems, cellulose is heated to a desired temperature in inert atmosphere, rapidly fragments and the resultant gaseous products are measured using analytical equipment, typically gas chromatographs couple to mass spectrometers. The subsequent

cellulose weight loss or final product yield data is then retroactively fitted to solve for kinetic parameters and create overall kinetic models. This approach frequently results in lumped kinetic models, such as the Broido-Shafizadeh mechanism, where specific product classes are "lumped" (e.g. gases, tars, char) to fit kinetic parameters.[45–47] Many models have been proposed with a variety of overall reaction schemes, but there is no consensus on a valid model as these models can have kinetic parameters differing by orders of magnitude.

There are numerous factors hindering the ability to obtain kinetic data and elucidating pyrolysis chemistry. First, the high temperatures required for cellulose pyrolysis (> 400°C) provide a greater amount of energy to break chemical bonds than is required for many of the proposed elementary reaction steps, making it challenging to narrow a list of possible reaction mechanisms. Second, pyrolysis product mixtures are quite complex and contain hundreds of various organic compounds that have a variety of chemical functionality.[6,48] Complete quantification of these mixtures through gas chromatography is analytically intensive; where proper quantification requires each product in the mixture to be identified and calibrated individually compared to standards that must be purchased, isolated or synthesized. This analytical challenge often leads to erroneous quantification of some products and leads to errors when measuring kinetic parameters. Third, pyrolysis is a rapid process with the reaction going to completion within a couple seconds. Thermogravimetric analyzers are really only suitable for slow pyrolysis (< 200 °C) as they can only heat samples with maximum heating rates of 200 °C/min, and only reach desired reaction temperatures by the time significant amount of reaction has already occurred.[49]

Additionally, the quick reaction times challenges the other main techniques as the analytical equipment coupled to these reactors require hours to perform the methods that quantify products during an experiment.[19] This mismatch of time-scales renders it impossible to obtain time resolved kinetic data, and thus intermediate chemical species cannot be identified or quantified with these techniques. The last challenge is experiments use cellulose powder samples whose thicknesses are on the order of millimeters. On these length scales, samples can exhibit large temperature gradients and induce additional secondary reactions when formed products diffuse from the sample, altering product distributions significantly.[19,50] Thus, kinetic data is often convoluted by these physical processes and requires methods to decouple heat and mass transfer from the intrinsic chemistry. New experimental techniques that overcome all of these challenges are required.

With improved experimental methods capable of measuring intrinsic kinetics, one of the more important reaction steps, the activation of cellulose, can be elucidated. Activation, sometimes referred to as initiation, has been heavily studied in the literature since comprehension of initial cellulose fragmentation will allow for some insight into the identity of the intermediate melt phase and how desired products are formed from this intermediate state.[15] Activation has been proposed to occur via heterolytic or homolytic radical cleavage, water catalyzed hydrolysis, concerted transglycosylation and many others.[28,39,51–53] Activation mechanisms have been proposed a wide range of kinetic parameters, with activation energies ranging from 10 – 240 kJ/mol and first-order kinetic frequency factors differing by orders of magnitude. This wide range of proposed kinetics clearly demonstrates how the complexity of pyrolysis hinders the ability to probe intrinsic

chemistry. The ability to properly elucidate this mechanism and others is dependent on obtaining proper intrinsic kinetic data.

An additional complication while studying cellulose pyrolysis chemistry and the initiation mechanism is the presence of inorganic metals in lignocellulosic biomass. These metals, in particular alkali and alkaline earth metals like potassium, calcium, and magnesium, behave as catalysts and alter cellulose pyrolysis product distributions significantly.[24,54–56] The majority of literature shows these metals increase the yield of char and light oxygenates and decrease the yield of anhydrosugars and furans. This result is undesirable for biofuels and chemicals production as bio-oil yield should be maximized. Studies examining weight loss data of cellulose impregnated with these metals observe catalytic effects on the initial decomposition of cellulose, where the temperature that maximum weight loss occurs at shifts to lower temperatures with the addition of metals.[57,58] Similar to non-catalyzed pyrolysis chemistry, catalytic chemical mechanisms are not accurately described and the role of these catalysts are solely based on differences in product yields. Useful intrinsic kinetic data would enable better understanding of the role of these metals, as any differences in the kinetics (e.g. activation energy or frequency factor) in the presence of these metals can be quantitatively discerned and changes in chemical mechanisms can be proposed. While most pundits believe these metals are an inhibitor on pyrolysis technologies and should be extracted from biomass before the process, only partial removal of these metals can be achieved with any economic chelating pre-treatment process and any removal is still an added cost to the process.[59] The lack of knowledge of how these metals alter pyrolysis chemistry still leaves the possibility that

these metals could promote a more desirable (e.g. more deoxygenated) bio-oil product and additional studies into their effects are required.

Therefore, this work will provide information of the effects that natural inorganic metals have on pyrolysis chemistry. The first part will focus on the recently developed reactor technique known as the Pulse Heated Analysis of Solid Reactions (PHASR), and its usefulness for studying cellulose pyrolysis chemistry. The next two sections will utilize this technique to study how calcium and magnesium, two naturally occurring alkaline earth metals in biomass, effect the initiation or thermal activation of cellulose during pyrolysis. This work will provide the first known mechanism that describes the role of these alkaline earth metals on activation, and will be supported by both experimental and computation evidence.

Chapter 3: Pulse Heated Analysis of Solid Reactions (PHASR)

3.1: Introduction

Previous attempts to elucidate the reaction kinetics of pyrolysis have led to inconsistent results that have been reactor and study specific. These inconsistencies are the direct result of the complexity of the fundamental processes involved in pyrolysis. The hundreds of chemical reactions occurring simultaneously with mass and heat transfer on a millisecond timescale convolutes the intrinsic reaction chemistry. Additionally, improper quantification of the products composing pyrolysis oils have led to further inconsistencies. Proper measurement of the reaction kinetics involved in cellulose pyrolysis requires new experimental techniques to overcome these challenges.

The development of three experimental techniques over the past nine years has greatly impacted the ability to measure kinetics for this complex process. The first of these is the advent of thin-film pyrolysis by Mettler et al.[19] In thin-film pyrolysis, cellulose samples are deposited inside the reactor as micron thick thin films as compared to the traditional powder samples that are on the order of millimeters. Micron thick samples increase the rate of heat and mass transfer by orders of magnitude allowing experimental results to only be controlled by the reaction chemistry. The second technique is the Quantitative Carbon Detector or Polyarc detector produced by Activated Research Company and is an add-on to flame ionization detector in gas chromatograms.[60–62] The Polyarc operates by taking all the individual carbon containing compounds of the reaction mixture upon separation by the chromatography column and

completely converting them individually to methane before their individual responses are measured by the flame ionization detector. Each compound can then be easily quantified by normalizing the detector response to the number of carbons each chemical species contains. This technique allows for reaction mixtures to be analyzed quickly and with improved accuracy as the only compound that must be calibrated is methane and methane has the most ideal response in flame ionization detectors preventing typical analytical errors when analyzing reaction mixtures. Maduskar et al. demonstrated the usefulness of this technique on analyzing pyrolysis oils in 2014.[60]

The third technique is the PHASR technique first demonstrated by Krumm et al. in 2016.[63] PHASR utilizes rapid thermal pulses of thin-film samples to control the reaction progress on a millisecond basis. This allows for the reaction to be sampled on the appropriate time scales, and temporally resolved kinetic data can be obtained. In this chapter, a more detailed assessment of the PHASR technique's efficacy for studying cellulose pyrolysis chemistry is provided. Five criteria to properly measure biomass kinetics are outlined and the ability of PHASR to satisfy these criteria are detailed.

3.2: PHASR Design

In the PHASR method, biomass samples are subjected to rapid thermal pulses of square waves with prescribed temperature and duration. The reactor incorporated millisecond heating and cooling of samples within a sealed vessel consisting of two parts as shown in Figure 3-1A: (i) an upper chamber with heating element, biomass sample, temperature measurement by optical pyrometry, and helium sweep gas flow, and (ii) a lower chamber with continuous flow of silicon-based coolant maintained at 3 ˚C. The reactor housing in the upper chamber includes electrical leads (pass-through copper wired) and a 1000 Hz optical temperature measurement, which form a control loop when integrated with a 2000 Hz PID controller as shown in Figure 3-1A. The upper and lower chambers were thermally connected using a composite layer of: (a) 250 μm copper microstructured heat exchange surface, (b) 250 μm aluminum nitride ceramic, and (c) 100 μm passivated steel resistive heating element. The unique design of PHASR reactor allows heating, temperature control, and cooling of thin film samples in millisecond timescale at the required reaction temperatures. A complete description of the PHASR device is available in prior work.[63]

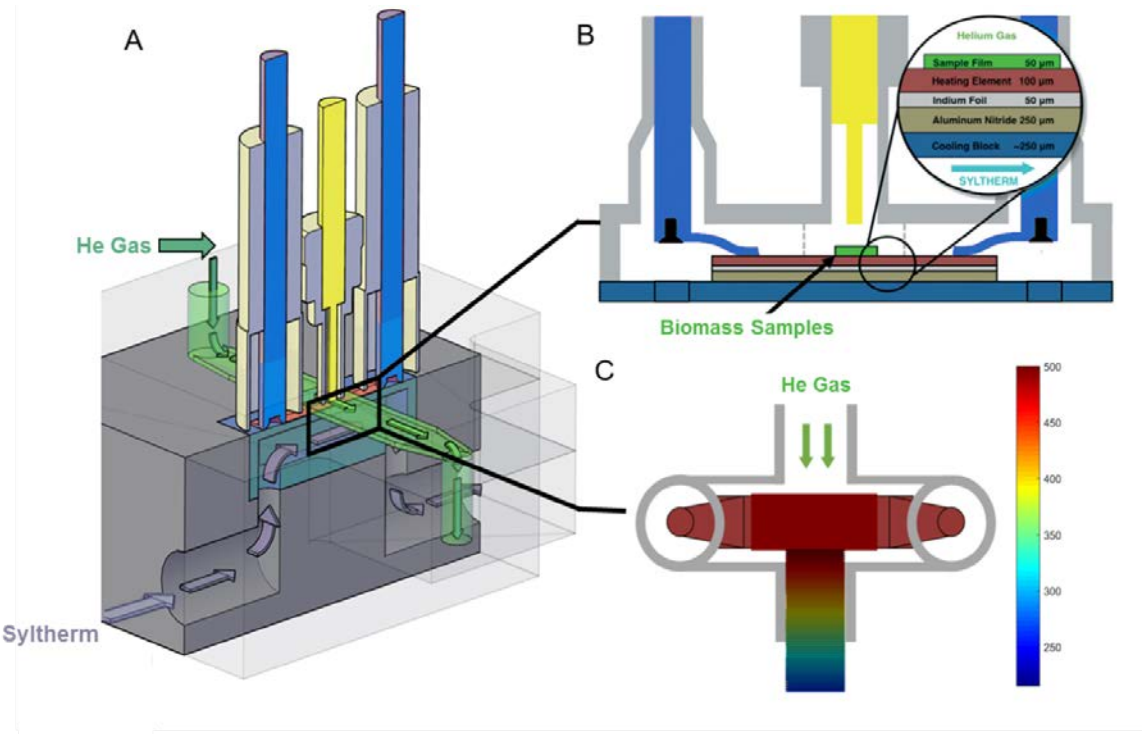

Figure 3-1. PHASR Reactor Design and Method. (A) Exploded diagram of the PHASR (pulse-heated analysis of solid reactions) system. Biomass film samples on a heating element are attached to electrical leads within a helium-flow chamber; gas/vapor effluent flows into a gas chromatograph. The lower chamber contains continuously flowing silicon-based coolant. (B) Gas flow chamber contains curved metal contacts connecting copper electrical leads and the heating element. Multiple layers of heating element, indium foil, aluminum nitride and a copper micro-channel cooling block transport heat between the gas and liquid chambers. Optical pyrometer in yellow measures the temperature at 1000 Hz. (C) Top-down view of the heating element and temperature map in the PHASR reactor. Vapor products are exposed to high temperature only above the heating element and lower temperatures downstream to minimize secondary reactions.

Reused with permission from Maduskar, S.; Facas, G. G.; Papageorgiou, C.; Williams, C. L.; Dauenhauer, P. J. Five Rules for Measuring Biomass Pyrolysis Rates: Pulse-Heated Analysis of Solid Reaction Kinetics of Lignocellulosic Biomass. ACS Sustain. Chem. Eng. ***2018***, 6 *(1), 1387–1399. Copyright 2018 Americal Chemical Society.* [50]

3.3: PHASR Evaluation for Measuring Pyrolysis Reaction Kinetics†

3.3.1: Small Biomass Length Scale

Biomass pyrolysis consists of a multi-phase, complex reaction network. Solid- and liquid-phase chemistries are convoluted with transport phenomena (conductive and convective heat transfer as well as liquid-phase diffusion).[64] It is necessary to conduct experiments with isothermal reacting samples devoid of heat and mass transport limitations. Mettler et al. illustrated this requirement by introducing reaction-transport diagrams, as shown in Figure 3-2, which compares the pyrolysis reaction rate with convective and conductive heat transfer rates via dimensionless quantities (pyrolysis numbers, Py^{I}, Py^{II} and Biot number, Bi). Py^{I} is the ratio of reaction and conduction time scales, Py^{II} compares of reaction and convection time scales, and Bi relates conduction and convection time scales. Pyrolysis experimental techniques traverse two reaction regimes by varying the characteristic length scale of the biomass samples at 500 ˚C.[15] For biomass particles, larger than one millimeter, the hot external surface reacts while the inside of the particle remains cold ($Py << 1$, $Bi >> 1$). For experiments utilizing biomass samples with characteristic lengths in the range of 10 μm to 1.0 mm, convection, conduction, and reaction rates are all within two orders of magnitude of one another. Therefore, thin film samples with characteristic length scale (film thickness) smaller than 10 μm are needed for studying isothermal reaction chemistry at pyrolysis temperatures.

† The work in this section was performed alongside Dr. Saurabh Maduskar.

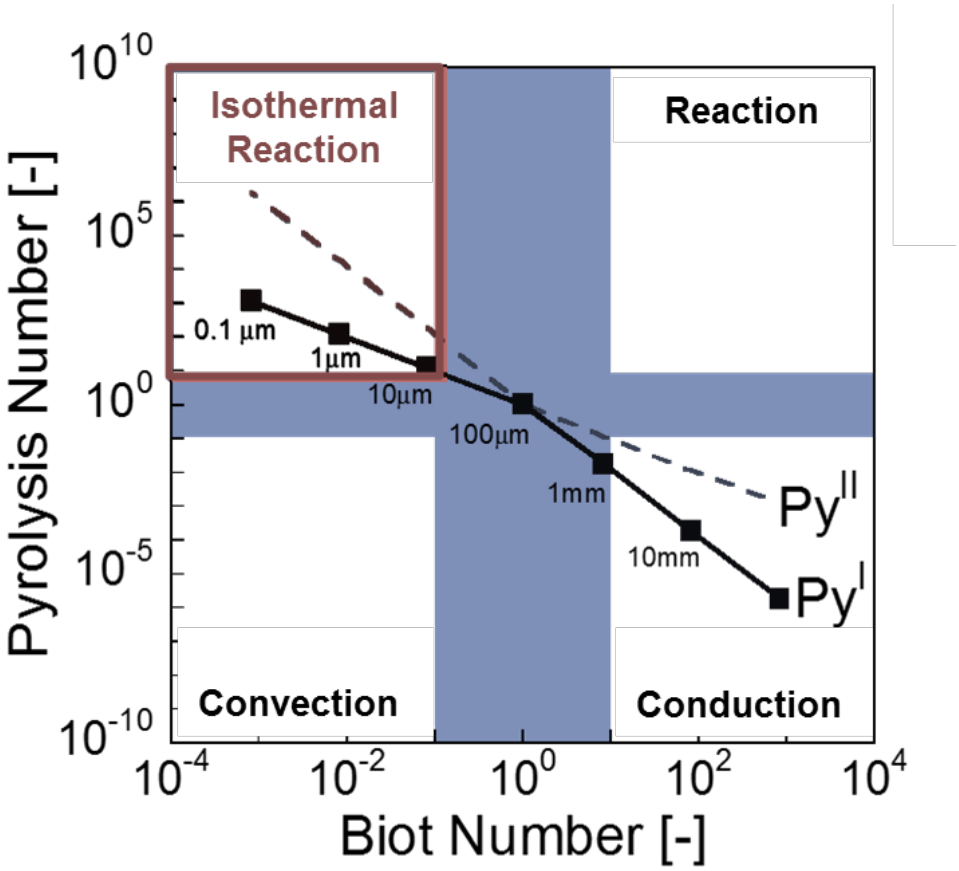

Figure 3-2. Pyrolysis Transport Map. Relative rates of biomass reaction and heat transfer by conduction or convection at 500 ˚C are compared in terms of Pyrolysis number and Biot number; four pyrolysis regimes are identified (clockwise from top left): isothermal and reaction-limited, reaction-limited, conduction-limited and convection-limited.

Reused with permission from Maduskar, S.; Facas, G. G.; Papageorgiou, C.; Williams, C. L.; Dauenhauer, P. J. Five Rules for Measuring Biomass Pyrolysis Rates: Pulse-Heated Analysis of Solid Reaction Kinetics of Lignocellulosic Biomass. ACS Sustain. Chem. Eng. ***2018***, 6 *(1), 1387–1399. Copyright 2018 Americal Chemical Society.*[50]

The requirement for short length scales on the order of tens of microns was demonstrated experimentally for cellulose pyrolysis chemistry. Long-chain cellulose polymer initially decomposes into shorter polymers and monomer products through primary reactions. These primary products further react in a liquid intermediate phase and

vapor phase through secondary reactions. By comparing product yields for powder (millimeter-sized non-isothermal samples which are transport-limited) and thin-film (micrometer-scale films which are isothermal) pyrolysis, it was shown that sample dimension drastically affects reaction pathways. For example, levoglucosan (the most abundant product of cellulose pyrolysis) yield differs significantly between conventional powder pyrolysis and thin-film pyrolysis (49% for powder; 27% for thin-film at 500 ˚C)[19,50]. The effect of sample length scale on reaction kinetics was further demonstrated by measuring pyrolysis reaction rates for product formation using PHASR with varying sample thickness.[63] For cellulose samples thicker than 70 μm, the formation rate of products at 500 ˚C was shown to steadily decrease as the sample thickness increased indicating heat transfer limitations.

3.3.2: Temperature Measurement and Thermal Control

Due to the significant variation in reaction rate due to small changes in temperature, measurement of biomass sample temperature and control is critical for kinetic analysis. For high temperature reactions, such as fast pyrolysis, sensitivity, response and location of temperature measurement must be appropriate to accurately capture reaction temperature. In addition, the method of temperature measurement should not impact reaction chemistry.

In experimental studies using a thermogravimetric analyzer (TGA), the biomass sample temperature is assumed to be the same as the heating source temperature. In a recent review article, Lédé has demonstrated that assuming biomass sample temperature to be the same as the heat source temperature may lead to considerable errors in kinetics

experiments.[65] In a conventional TGA, the temperature difference between the heat source and biomass sample significantly increases with heating rate and can theoretically be as large as 100 ˚K.[65] In other commercial micro-reactor systems, such as a furnace pyrolyzer (Frontier Laboratories) and filament pyrolyzer (CDS analytical), sample temperature cannot be measured directly, and it is assumed that the biomass sample temperature matches the furnace/coil heating source temperature. The inability to directly monitor reaction temperature has led to several methods of approximation of effective reaction temperature which can lead to uncertainties in kinetic analysis.[66]

The PHASR and wire-mesh reactors both use an optical pyrometer to monitor reaction temperature.[44,63] This method is fast (response time 180 μs) and enables temperature measurement at a targeted spot of a biomass sample. In addition, this method was shown to be unaffected by the presence of pyrolysis vapors and aerosols generated during reaction.[67] In the case of the wire-mesh reactor, the biomass sample distribution on the mesh was found to significantly affect temperature gradient in the sample. Even with a uniform distribution of biomass over the entire mesh surface, temperature was found to fluctuate as much as 35 ˚C.[44] Given the temperature sensitivity of the pyrolysis reaction, this variation can induce significant error in kinetic measurements. In the PHASR reactor, uniform deposition of thin-film samples of biomass on smooth, highly conductive heating elements of carbon steel leads to negligible temperature variation across a sample; this design leads to an accurate temperature measurement within ± 3 ˚C. In addition, the PHASR reactor has a millisecond temperature control loop. A high frequency pyrometer (1000 Hz) coupled with high frequency PID controlled power supply (2000 Hz) can control

heating pulse and reaction progression at the millisecond time scale. By this design, the control system responds at least an order of magnitude faster than the reaction.

3.3.3 Temperature Ramp during Heating

To develop an accurate measurement of pyrolysis reaction kinetics, the extent of conversion of the biomass sample during the heating and cooling time should be negligible as compared to the extent of reaction during the isothermal reaction time period.

For a given chemical reaction with known kinetic parameters, the minimum temperature ramp required (H [=] $K \cdot sec^{-1}$) can be calculated at a specific reaction temperature such that total conversion during heating and cooling is minimal (<5 %). Differential conversion dx during heating for a first order reaction can be defined as,

$$\frac{dx}{(1-x)} = A\exp\left\{-\frac{E_a}{R(T_o + Ht)}\right\}dt \qquad (3\text{-}1)$$

where A is the Arrhenius pre-exponential factor; E_a is activation energy; R is universal gas constant; T_o is initial temperature (room temperature); H is temperature ramp in (K/sec), and t is time in seconds. Integrating equation (1) from $t = 0$ to $t = \frac{(T_{reaction} - T_o)}{H}$, the required value of H for a given $T_{reaction}$ such that conversion $x \leq 5\%$ can be obtained. Using the kinetics of conversion of α-cyclodextrin, a known cellulose surrogate as shown in Figure 3-3, the linear thermal ramp during heating required for limited conversion is calculated from Figure 3-4A for relevant target reaction temperatures (410 < T < 530 ˚C).[68] To study biomass reactions occurring at 500 ˚C, the linear temperature ramp of a solid lignocellulose sample must be faster than 7250 ˚C/sec.

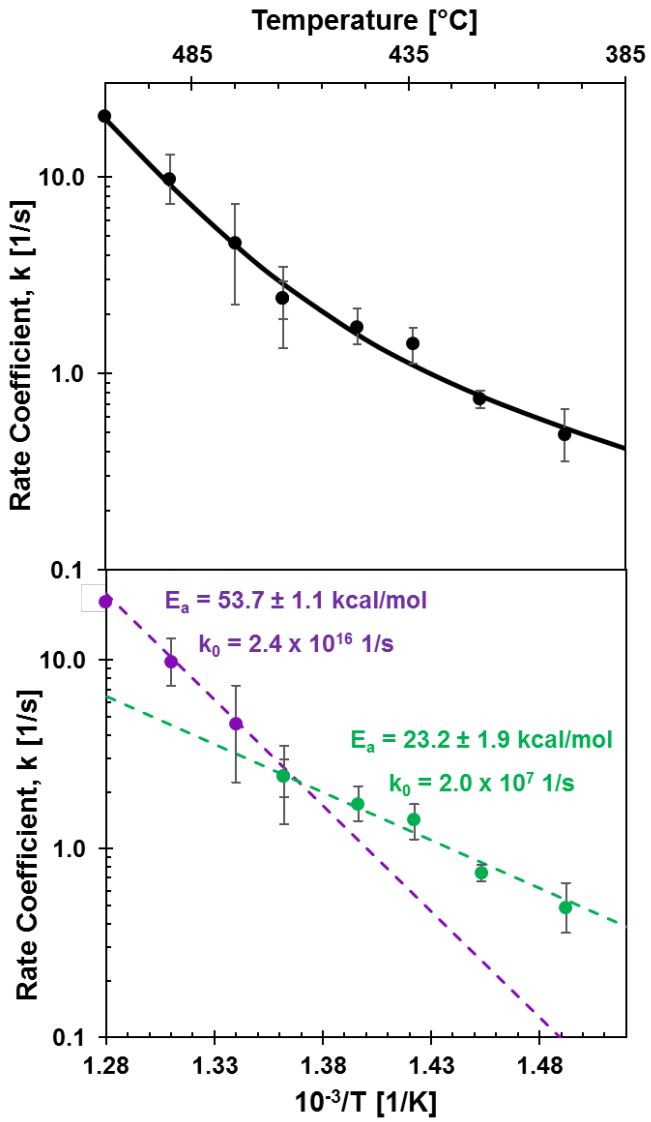

Figure 3-3. Kinetics of Cellulose Activation. Data points indicate the first order rate coefficient of the conversion of cellulose surrogate α-cyclodextrin at varying temperature. The conversion of α-cyclodextrin exhibits two kinetic regimes with a transition point around 467 ˚C, indicative of a change in the mechanism of glycosidic bond cleavage. Error in the apparent activation energy represents a 90% confidence interval.

Reused with permission from Maduskar, S.; Facas, G. G.; Papageorgiou, C.; Williams, C. L.; Dauenhauer, P. J. Five Rules for Measuring Biomass Pyrolysis Rates: Pulse-Heated Analysis of Solid Reaction Kinetics of Lignocellulosic Biomass. ACS Sustain. Chem. Eng. ***2018***, 6 *(1), 1387–1399. Copyright 2018 Americal Chemical Society.*[50]

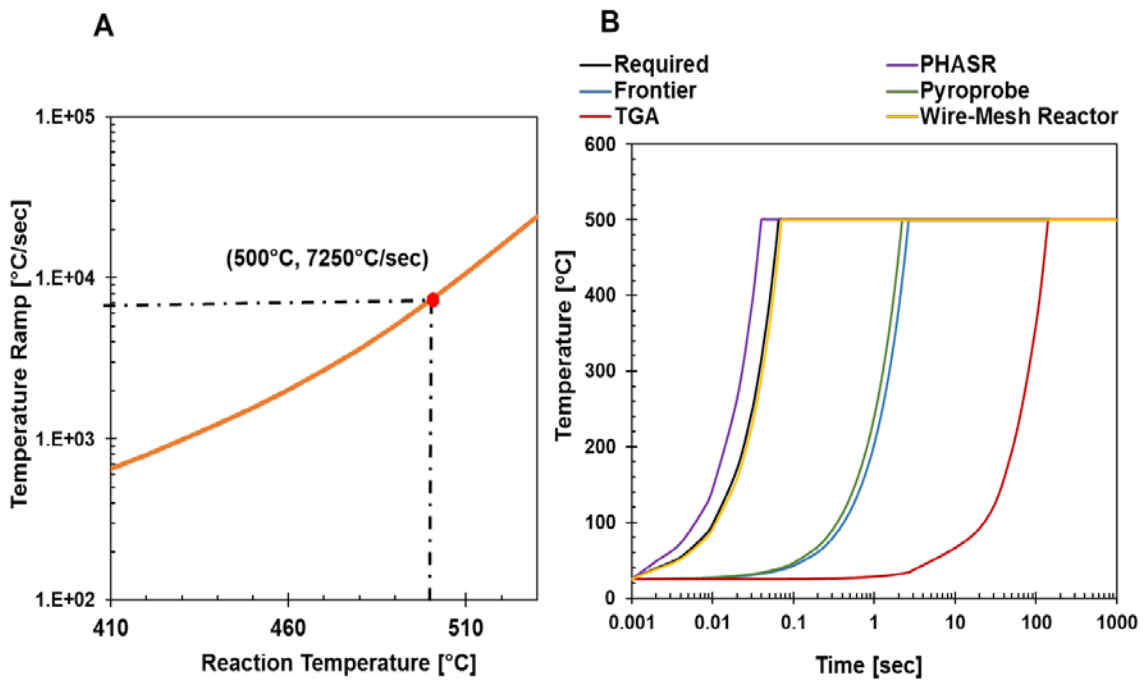

Figure 3-4. Required Heating Rate for Biomass Sample Pyrolysis. (A) Required temperature ramp during heating at a given reaction temperature with negligible conversion ($x \leq 5\%$) calculated by equation 3-1. (B) Comparison of biomass sample temperature profile during heating in different pyrolysis reactors.

Reused with permission from Maduskar, S.; Facas, G. G.; Papageorgiou, C.; Williams, C. L.; Dauenhauer, P. J. Five Rules for Measuring Biomass Pyrolysis Rates: Pulse-Heated Analysis of Solid Reaction Kinetics of Lignocellulosic Biomass. ACS Sustain. Chem. Eng. ***2018***, 6 *(1), 1387–1399. Copyright 2018 Americal Chemical Society.* [50]

Figure 3-4B compares heating temperature profile of various biomass pyrolysis reactors from $T_o = 25$ ˚C to $T_{reaction} = 500$˚C. Thermogravimetric analyzers (TGA) can attain a maximum heating ramp (in red) of 200 ˚C/min, which is three order of magnitude lower than the required heating rate (in black). To characterize the Frontier micropyrolyzer, thermal measurement combined with computational fluid dynamics modeling of the gas flows within the reactor drop-tube furnace was used to determine a maximum temperature

ramp of the reactor cup of 200 ˚C/sec.[69] In a similar study evaluating the filament pyrolyzer CDS Pyroprobe 5000, which allows the user to set the nominal heating rate to 20 ˚C/ms (20,000 ˚C/s) on the platinum coil, it was found that the heating rate does not represent the heating rate on the sample itself. For a heating rate set point of 20,000 ˚C/s (in the coil), the fastest measured heating rate at sample center was 216.4 ˚C/s and the average heating rate was around 131.1 ˚C/s at atmospheric pressure.[70,71] As depicted in Figure 3-4B, these effective sample thermal ramping rates for Frontier micropyrolyzer (in blue) and CDS pyroprobe (in green) are significantly lower than the required temperature ramp and heating rates. The effective heating rates in resistively-heated wire-mesh (in yellow) and PHASR (in violet) reactor systems are comparable to the required heating rates.

Table 3-1 lists experimental reactors used to study biomass pyrolysis and the measured thermal ramp during heating. The maximum operating temperatures meeting this requirement for different systems are well below the pyrolysis temperature, which suggests that at high temperatures significant portion of the overall conversion occurs at a lower temperature than the final desired temperature.

Table 3-1. Pyrolysis Reactor Performance and Thermal Limitations. Four fast pyrolysis reactors (TGA - thermogravimetric analysis, the Frontier Micropyrolyzer, Pyroprobe, and PHASR - Pulse-Heated Analysis of Solid Reactions) expose a sample to a heating ramp rate. The "suitable temperature" is the maximum temperature below which negligible reaction of the biomass sample occurs during the heating phase.

Technique	Heating Ramp Rate [˚C/sec]	Suitable Temperature [˚C]
TGA	3.34	<212
Frontier	180	<351
Pyroprobe	216.4	<359
PHASR	15,800	<521

3.3.4 Online Detection and Temperature Ramp during Cooling

Measurement of the reaction kinetics of solid particles requires the ability to track the progression of reaction with time. While most experimental reactor systems conducting pyrolysis chemistry only allow reactions to progress to temporally characterize gas and vapor pyrolysis products. By the first method of 'online detection,' a pyrolysis reactor is coupled with an online analytical technique such as mass spectrometry; the evolving distribution of chemical species is then quantified in real time. An alternative method quenches the reacting solid sample, thereby limiting the extent of conversion to a pre-set time interval.

For either experimental method, the integrity of the experimental data relies on the ability to effectively measure the time-resolved composition of evolving product species. For the online detection method, the complex evolution of organic vapors and gases must be transferred from the pyrolysis reactor to the detector without significant mixing.

Alternatively, experimental methods that quench a reacting solid must cool sufficiently fast to prevent significant low temperature chemistry. Due to the existence of two different experimental methods, the fourth requirement is split into two alternative restrictions, 4A and 4B.

Requirement #4A: Online detection. The challenge associated with online pyrolysis characterization arises from the combination of a pyrolysis reactor with an analytical system capable of quantifying the evolving chemical mixtures. As depicted in Figure 3-5, the time scales of reaction and chemical analysis can be compared for common techniques. While many changes occur on the order of seconds or kiloseconds with conventional heterogeneous catalytic systems, the transient nature of particle pyrolysis occurs in milliseconds. With regards to chemical analysis, gas and liquid chromatography are capable of separating, identifying, and quantifying complex mixtures arising from pyrolysis, but they are too slow (τ_{GC} ~ ks) to couple with reacting biopolymers. Spectroscopic techniques such as infrared, UV/visible, or nuclear magnetic resonance are faster (τ_{spec} ~ s), but they are incapable of resolving and quantifying 10-100 simultaneous organic compounds. Mass spectrometry techniques such as TOF-MS approaches the time scales of pyrolysis (τ_{MS} ~ 50 ms), but it is incapable of scanning a sufficient mass-to-charge (m/z) range at this rate to quantify 50+ organic compounds evolving over 10-50 milliseconds.

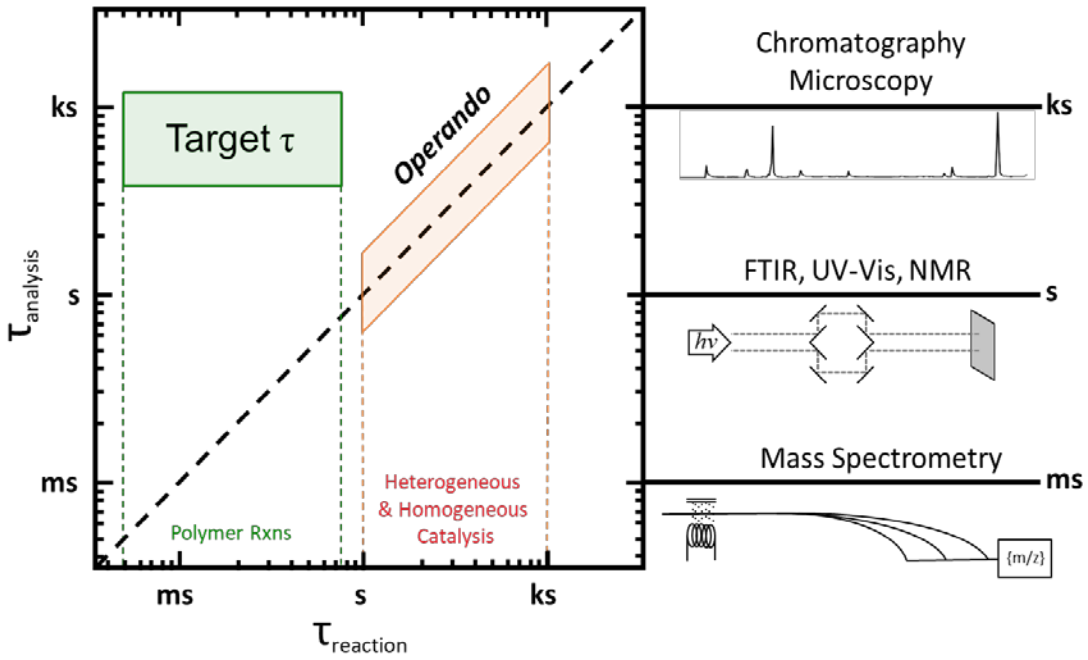

Figure 3-5. Disparity in time scales of polymer reactions (in milliseconds) and conventional analytical techniques (in seconds and kiloseconds) underscores the need of reaction quench at the millisecond time scale.

Reused with permission from Maduskar, S.; Facas, G. G.; Papageorgiou, C.; Williams, C. L.; Dauenhauer, P. J. Five Rules for Measuring Biomass Pyrolysis Rates: Pulse-Heated Analysis of Solid Reaction Kinetics of Lignocellulosic Biomass. ACS Sustain. Chem. Eng. ***2018***, 6 *(1), 1387–1399. Copyright 2018 Americal Chemical Society.*[50]

Temporal characterization of the pyrolysis of biomass can potentially be implemented by combining a high temperature flow reactor with online mass spectrometry (τ_{MS} ~ 10 ms) as shown in Figure 3-6A, provided the time-resolved reactor effluent stream does not mix prior to characterization. This system exhibits three rates relevant to the characterization process: (a) the rate of volatile product formation, (b) the rate of sample mixing, and (c) the rate of transfer between the reactor and the detector. If the rate of volatile product formation and the rate of transfer between reactor and detector is significantly greater than the rate of mixing, the detector will temporally-resolve a

composition stream comparable to the rate of reaction. Integrity of the temporal composition stream from the reactor to the detector can be characterized via dimensional analysis. Figure 3-6B compares relative rates of the three processes in terms of ratios of characteristic time constants of reaction to diffusion (x-axis) versus transfer to diffusion (y-axis). The relative rates of the system will depend on reaction characteristics (*k*, *D*), and design parameters (*l, u*), where k is the pyrolysis reaction rate coefficient, D is the axial diffusion coefficient, l is the length of the transfer tube, and u is the velocity of the fluid in the transfer tube. The time scale of reaction, τ_{rxn}, is characterized by the inverse of the rate coefficient, k [=] s^{-1}. Solid reactions exhibit complex kinetics which can be approximated as zero, first, or second order systems. Cellulose has been shown to exhibit both first and zero order of furan formation kinetics, with measured rate parameters for initiation reaction as $0.3 < k < 20\ s^{-1}$ for $380 < T < 500$ ºC corresponding to $0.05 < \tau_{rxn} < 3.3$.

The residence time of the transfer between the reactor and detector, $\tau_{res} = l \cdot u^{-1}$, is calculated as the transfer line length, *l*, divided by the transfer fluid (e.g. helium) velocity, *u*.

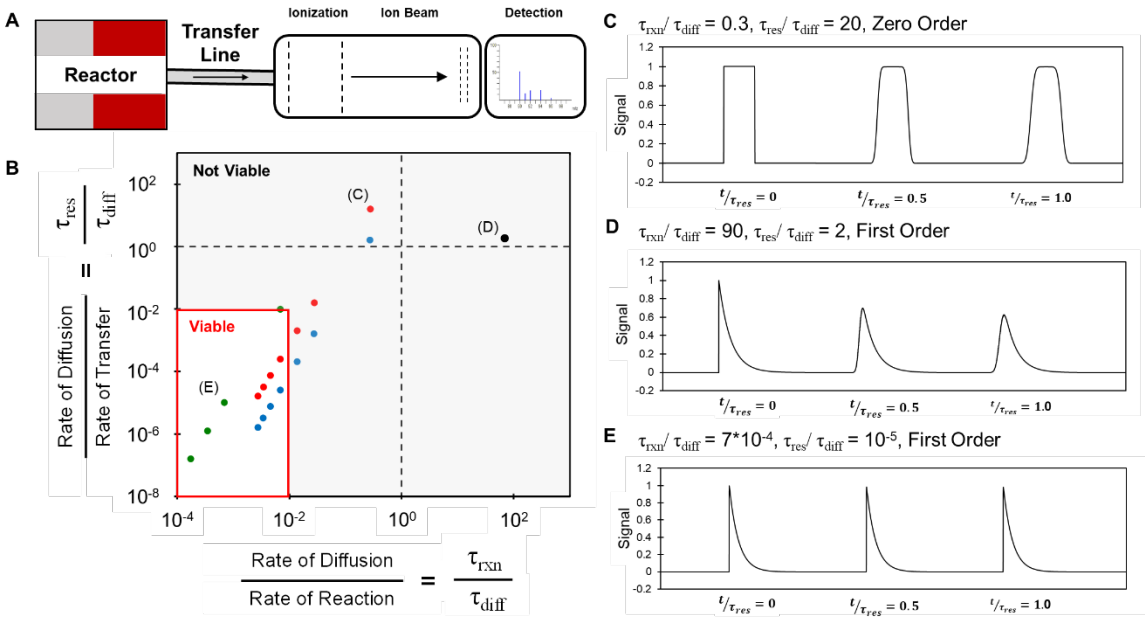

Figure 3-6. Design Requirement for a Reaction-Detector Coupled System. (A) Schematic of high temperature pyrolysis reactor with online mass spectrometry. (B) Comparison of relative time scales of diffusion and residence time within the transfer line (τ_{res}/τ_{diff}) versus diffusion in the transfer line and reaction rate in the reactor (τ_{rxn}/τ_{diff}). The viable region corresponds to the operating conditions such that the rate of diffusion is at least two orders of magnitude lower than both rate of reaction and rate of product transfer between the reactor and detector. Operating points are selected for different reaction and design parameters as described in the supporting information (Table 3-2). (C) Simulated detector signal for a non-viable operating point C for a zero-order reaction profile. (D) Simulated detector signal for a non-viable operating point D for a first-order reaction profile (E) Simulated detector signal for a viable operating point E for a first-order reaction profile.

Reused with permission from Maduskar, S.; Facas, G. G.; Papageorgiou, C.; Williams, C. L.; Dauenhauer, P. J. Five Rules for Measuring Biomass Pyrolysis Rates: Pulse-Heated Analysis of Solid Reaction Kinetics of Lignocellulosic Biomass. ACS Sustain. Chem. Eng. ***2018***, 6 *(1), 1387–1399. Copyright 2018 Americal Chemical Society.*[50]

Mixing of the temporally-evolving sample of organic products from pyrolysis can occur within the reactor, at the reactor exit, within a tubular transfer line, and at the inlet to the detector. The extent of mixing can be estimated as axial diffusion of vapors within inert gases transferred between the reactor and the detector using diffusion coefficient $D \sim 1 \cdot 10^{-}$

[5] m^2sec^{-1}. The time constant of mixing, $\tau_{diff} = L_c^2 \cdot D^{-1}$, can then be calculated as the ratio of the square of the characteristic length, L_c, divided by the diffusivity, D. The characteristic length of the evolving organic sample is calculated as $L_c = u \cdot k^{-1}$ (for a first order reaction), such that the time constant of mixing is calculated as $\tau_{diff} = u^2 \cdot D^{-1} \cdot k^{-2}$. A zero order reaction has a characteristic length of the evolving organic sample calculated as $L_c = u \cdot k^{-1} \cdot C_0^{-1}$.

The region of viable operation was identified in Figure 3-6B such that rate of diffusion is at least two orders of magnitude lower than both rate of reaction and rate of product transfer.

A set of experimental and reaction conditions (*D, u, l, k*) correspond to an operating point on Figure 3-6B with coordinates of corresponding relative rates. It is evident from the trend in Figure 3-6B that the operating point can traverse from 'non-viable' to 'viable' region by decreasing transfer line length (*l*) and increasing velocity (*u*). Each of the operating points on Figure 3-6B can be calculated from the values of experimental operating conditions (*u*,*l*) and reaction parameters (*k, D*). It should be noted that *D* also depends on temperature and pressure in the transfer line.

- Red series of operating points was generated using following conditions: $D = 1 \cdot 10^{-5}$ $m^2.sec^{-1}$, $k = 12$ sec^{-1}, $l = 1 \cdot 10^{-1}$, and $u = 0.02$ to 2 m/sec (For example, 10-100 ml/min flow in 1/8" tube).
- Blue series of operating points was generated using following conditions: $D = 1 \cdot 10^{-5}$ $m^2.sec^{-1}$, $k = 12$ sec^{-1}, $l = 1 \cdot 10^{-2}$, and $u = 0.02$ to 2 m/sec (For example, 10-100 ml/min flow in 1/8" tube).

- Green series of operating points was generated using following conditions: D = $1 \cdot 10^{-5}$ $m^2 \cdot sec^{-1}$, k = 0.3 sec^{-1}, l = $1 \cdot 10^{-1}$, and u = 0.02 to 2 m/sec (For example, 10-100 ml/min flow in 1/8" tube).

Three different operating points (C, D, and E) were chosen with the conditions in Table 3-2 for simulating the observed response of the detector. Simulated response was calculated by solving the diffusion equation for plug flow in a pipe with axial diffusion, D, for the given initial conditions (e.g. first order, zero order at time zero).

Table 3-2. Experimental Conditions and Reaction Parameters used to Calculate Operating Points.

Point	Diffusion Coefficient, D $m^2 \cdot sec^{-1}$	Velocity, u $m \cdot sec^{-1}$	Transfer line length, l m	First order reaction rate constant, sec^{-1}
C	$1 \cdot 10^{-5}$	$2 \cdot 10^{-2}$	$1 \cdot 10^{-1}$	12*
D	$5 \cdot 10^{-5}$	$2 \cdot 10^{-2}$	$1 \cdot 10^{-1}$	12
E	$1 \cdot 10^{-5}$	$1 \cdot 10^{-2}$	$1 \cdot 10^{-1}$	0.3

* Assumes $C_0 = 1$

Figure 3-6C, D, and E depict a simulated response of an online mass spectrometer corresponding to different experimental conditions. Experimental condition points C and D fall in the 'non-viable' region and lead to a corrupted compositional profile. For the experimental conditions of point E with viable operating parameters, the reaction profile is retained.

Mixing of the temporally-produced composition profile can derive from many sources and limit the capability of online chemical detection techniques. Composition profiles mix within the reactor, upon the entrance to a sample transfer line, within a transfer line, and at the exit of the transfer line. As depicted in Figure 3-6C and D, even minimal mixing can

significantly corrupt a kinetic measurement. In particular, sharp transitions in concentration resulting from either zero order (3-6C) or first order (3-6D) pyrolysis kinetics rapidly mix with the carrier gas (e.g. helium) and reduce the value of the initial reaction rate. Due to the challenge associated with mixing combined with the requirement of fast chemical characterization, direct coupling of fast pyrolysis at 500 ˚C (τ_{rxn} ~ 10 ms) with online chemical analysis is not well suited for the analysis of complex chemical mixtures that evolve faster than the current detection rate.

Requirement #4B: Temperature ramp during cooling (cooling rate). Temporal analysis of pyrolysis products becomes feasible with analytical pyrolysis reactors that have an additional reaction quench process. By stopping the solid chemistry at short time scales, the resulting product gases, vapors, and solid residue (i.e. char) can be characterized with extent of reaction (i.e. time), provided the quench is sufficiently fast. This approach decouples the time scale of reaction (millisecond) from the time scale of analysis (kiloseconds for chromatography).

The required temperature ramp during cooling (i.e. cooling rate) can be identified as the rate that results in negligible feedstock conversion during the quench process. This rate is calculated for a given solid pyrolysis reaction using the method of equation 1. Figure 3-7A shows the required thermal ramp rates during cooling for cellulose pyrolysis at relevant reaction temperatures (400-530 ˚C). Calculations used kinetic parameters previously measured with cellulose conversion kinetics.[68] It should be noted that the minimum required cooling rate decreases as the reaction progresses due to a decrease in reaction rate with increase in conversion. From Figure 3-7A, it is apparent that the required cooling rate

for cellulose that has already achieved 30% conversion is higher than that of cellulose that has already achieved 40% conversion. Also, at 0% conversion, the required cooling rate is identical to the required heating rate at a given reaction temperature.

Figure 3-7B compares temperature profiles during cooling for different reactors from *Treaction* = 500˚C to *To* = 25 ˚C. The convective cooling rate achieved with carrier gas in TGA (not shown) and wire-mesh reactors (in red) are extremely low as compared to the required cooling rate for *Treaction* = 500 ˚C at 30% conversion (in black). In a Frontier micropyrolyzer, the reaction mixture can be cooled using compressed air or Nitrogen circulating through a metallic tube around the furnace tube. The reported cooling rate of 30 minutes from 600 ˚C to 50 ˚C (in red) is four orders of magnitude lower as compared to required cooling rate.[72] The PHASR system uses high velocity Syltherm heat transfer fluid circulating through a micro-heat exchanger directly in contact with the sample. This unique feature of PHASR enables rapid cooling rates (in violet) which are comparable to the required cooling rate (in black).

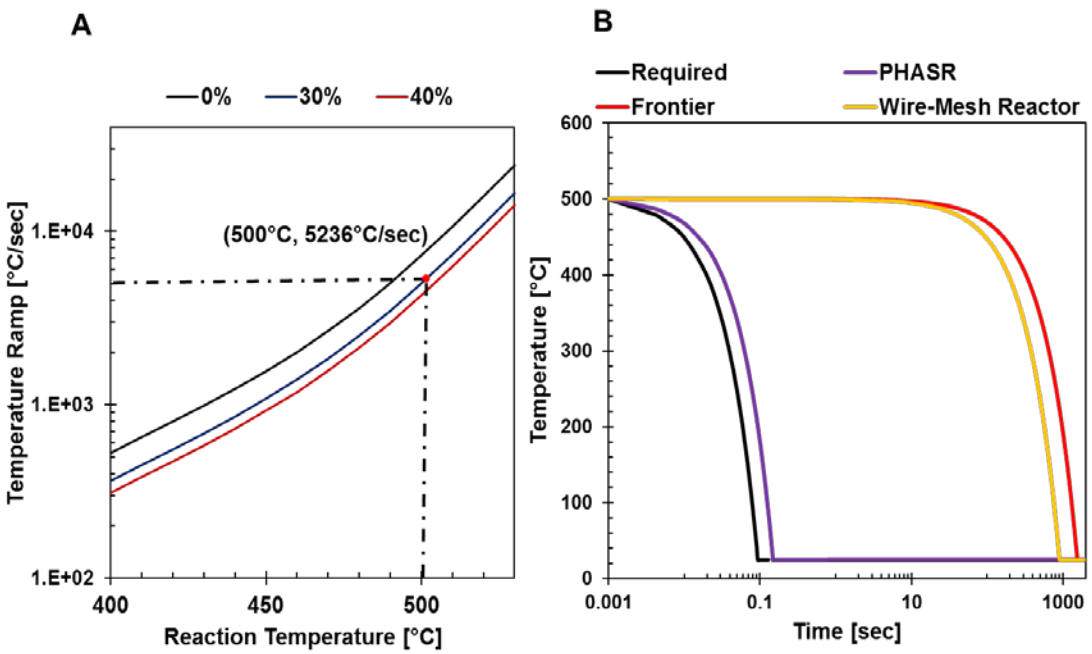

Figure 3-7. Cooling Rate Requirement of Kinetic Biomass Pyrolysis Reactor. (A) Required temperature ramp during cooling, at a given reaction temperature and conversion, to achieve negligible conversion during cooling ($x \leq 5\%$) calculated by equation 3-1. (B) Comparison of biomass sample temperature profile during cooling in different pyrolysis reactors.

Reused with permission from Maduskar, S.; Facas, G. G.; Papageorgiou, C.; Williams, C. L.; Dauenhauer, P. J. Five Rules for Measuring Biomass Pyrolysis Rates: Pulse-Heated Analysis of Solid Reaction Kinetics of Lignocellulosic Biomass. ACS Sustain. Chem. Eng. ***2018***, 6 *(1), 1387–1399. Copyright 2018 Americal Chemical Society.*[50]

3.3.5 Sweep Gas Flow Rate

In the complex reaction network of cellulose thermal degradation primary products formed by glycosidic bond cleavage can evaporate or undergo secondary reactions in the intermediate liquid phase to new volatile vapor products. Additionally, the volatile products can further undergo degradation in the vapor phase through gas-phase reactions. Secondary reactions in the intermediate liquid phase can be eliminated by using thin film

samples. Thin film samples (< 70 microns) allow for volatile products to diffuse to the melt-gas interface and evaporate at least an order of magnitude faster than the rate of melt phase reactions; thus, the reaction rate becomes constant as all volatile products are produced only via the primary reaction pathways.

To minimize the vapor phase reactions, the reactor sweep gas flow rate should be sufficiently high to reduce residence time of vapor products. Residence time of vapors in the furnace-type Frontier micropyrolyzer was experimentally measured using iodine crystal volatilization.[69] Based on visual observation, it was found that vapor residence time can be as high as 85 seconds, which will lead to vapor phase reactions during pyrolysis experiments. The residence time was found to be dependent on geometry and type of sample cup holder.

The PHASR microreactor was designed to eliminate mixing, and gas flows and chamber design enable laminar flow with low residence times. For the selected sweep gas flow rates and the PHASR microreactor volume, the residence time of the flowing helium used to entrain volatile products across the heating element was fewer than 10 milliseconds. Laminar flow ensures that entrained volatile organic products only flow to the reactor exit. Additionally, the use of a heating element distinct from the reactor body ensures that the sweep gases and entrained vapors are not exposed to the maximum reaction temperature. As depicted in the temperature map of PHASR in Figure 3-1C, vapor products are exposed to high temperature only above heating elements and are exposed to lower temperatures downstream which minimizes secondary reactions. At the same time the downstream temperature is high enough to avoid condensation of high molecular weight products.

In this chapter, five requirements for measuring biomass pyrolysis kinetics were identified as: a short sample length scale, fast heating and cooling rates (or minimal sample mixing for online detection), direct thermal measurement and control, and high product sweep gas flow rate. Performance of five different analytical pyrolysis reactors was compared with respect to the required criteria for each of the identified parameters. As depicted in Table 3-3, the PHASR technique demonstrated capability for achieving all five design criteria relative to other conventional reactors and is the most suitable for reaction kinetic measurements of biomass pyrolysis.

Table 3-3. Characteristics of High Temperature Biomass Pyrolysis Reactors.

Pyrolysis Reactors	Sample Length	Heating Rate (˚C /sec)	Cooling Rate (˚C /sec)	Temperature Measurement	Gas-Phase Residence Time
Requirement	10-100 microns	7250	5236	Rapid, Direct	Milliseconds
Thermogravimetric Analyzer	millimeter	3.34	-	Slow, Indirect	Seconds
Frontier Micropyrolyzer	millimeter	180	0.31	Slow, Indirect	Seconds
Pyroprobe	millimeter	216.4	-	Slow, Indirect	Seconds
PHASR	< 70 microns	11875	3167	Fast, Direct	10 ms
Wire-Mesh Reactor	millimeter	6600	0.52	Fast, Direct	milliseconds

Chapter 4: Calcium Assisted Activation of Cellulose

4.1: Introduction

Thermochemical conversion of biopolymers such as cellulose, composed of long linear chains of D-glucose units connected by β-(1,4)-glycosidic linkages, is a promising route to renewably produce an array of C5-C6 oxygenates that can be catalytically upgraded to fuels and chemicals.[6,10,27] Fast pyrolysis is one such thermochemical conversion technology, wherein cellulose rapidly fragments into gases, monomers (such as levoglucosan), char, and light oxygenates at temperature between 400-600 °C.[2,14,26,73] While fundamental insight into the molecular transformations of lignocellulose is critical towards further optimization of pyrolysis, detailed chemical insight remains in its nascent stages. The lack of sufficient progress in fundamental insight can be attributed to the dual-challenge of: (1) describing the transformation over the short time scales (milliseconds) over which pyrolytic reactions occur, and (2) the complex macromolecular structure of the feedstock and resulting mixture of products.[15,49,74] This complexity not only makes it particularly difficult to quantify the conversion of cellulose but also presents problems in building realistic computational models to probe proposed mechanisms.

Challenging lignocellulosic feedstocks also have varying amounts of alkaline earth and alkali metals, such as calcium, magnesium & sodium, which chemically influence the composition of the final product yields and the overall rate of cellulose breakdown.[24,55,75,76] Little is known of the mechanisms by which these natural metal catalysts interact and accelerate chemical pathways in cellulose decomposition. Existing studies focusing on catalyzed breakdown use thermal analysis techniques such as TGA and DSC to show that

these metals reduce the onset temperature where cellulose degradation occurs in addition to reducing the temperature where maximum degradation occurs.[57,77] There remains a clear need for a deeper understanding into the mechanisms and catalytic roles of these metals.

While the techniques discussed herein can be applied to studying any part of the cellulose reaction network, the initial step of glycosidic bond activation is the focus of this this chapter due to its key role in determining the overall rate of conversion and the final product speciation.[45,78] Moving towards a more detailed, molecular-level understanding of activation kinetics requires a combination of experimental and computational techniques that are capable of addressing the dual challenges of short reaction timescales and complex macrostructures. Previous experimental studies use product yield data from heat-transfer-limited experiments at complete conversion to fit kinetic parameters for a proposed chemical mechanism.[32,46,79] However, this approach does not include information on individual reaction pathways in addition to the kinetics of cellulose conversion and product evolution, thereby requiring complex reaction models to rely entirely on a large number of computed kinetic parameters that cannot be experimentally validated.[47] Alternatively, the microreactor Pulse Heated Analysis of Solid Reactions (PHASR) was developed by Krumm et al. using a combination of thin film techniques and rapid pulse heating/cooling to start and stop reactions with a temporal resolution as small as 20 milliseconds.[63] As shown by previous experiments, PHASR provides temporally-resolved reaction kinetic data absent heat and diffusion transport artefacts, thereby permitting direct comparison between experimentally-measured reaction rates and computed mechanisms.[49,50,63]

Accounting for complex structures of the feedstock is an issue receiving increased attention with the advent of increased computational resources to perform quantum chemical calculations.[80] Hosoya et al. were one of the first to show that accounting for complex H-bonding networks that arise out of the crystalline structure of cellulose Iβ can lead to increases in activation barriers by almost 10 kcal/mol.[39] Seshadri et al. have also shown that small alcohols and water could potentially interact with these complex feedstocks during pyrolysis and aid in reaction.[81] In addition to these penalties to the activation barrier, recent studies have also shown that new catalyzed pathways for cellulose activation can exist at lower temperatures (<467 C) due to the unique catalytic role of vicinal hydroxyl groups in the cellulose matrix.[68,82] These features of pyrolytic chemistry are not accounted for with simple reaction models and can only be probed via the use of explicit modeling of the environment surrounding the reacting cellulose chains. More specifically, if one considers the binding of metal ions to different parts of the cellulose matrix, the degree of complexity in the models will not only dictate the location of stable binding sites, and hence influence catalysis, but also secondary effects such as re-organization of H-bonding networks. These metal-driven phenomena and their effect on the surrounding reaction environment can be modeled using explicit cellulose sheets.

In this work, the conversion kinetics of α-cyclodextrin (CD), a known cellulose kinetic surrogate, were measured using PHASR in the presence of calcium, one of the natural metal cations known to accelerate cellulose decomposition kinetics.[19] The PHASR microreactor allowed for the generation of time-resolved conversion data of α-cyclodextrin at varying temperatures (370-430 °C) and calcium concentrations (0.1-0.5 mmol/g CD).

Using the time resolved conversion data, the kinetics for calcium catalyzed cellulose activation were fit to reveal the energetics for metal-catalyzed cleavage of glycosidic bonds. In conjunction with these experimental studies, first principles density functional theory (DFT) calculations were performed to identify favorable metal binding positions as well as nature of the active sites. Various mechanisms were evaluated where up to two calcium ions can participate in the cleaving of glycosidic bonds. This allowed for the elucidation of the primary catalytic role of calcium as well as a secondary role that calcium contributes in disrupting H-bonding networks and thus influencing kinetics. This chapter presents the first such study on intrinsic cellulose activation kinetics in the presence of metal salts and sheds light on the unique roles that metal ions can play in enhancing reactivity.

4.2: α-Cyclodextrin as a Kinetic Surrogate for Cellulose

Measuring the kinetics of activation of cellulose requires the capability to monitor the conversion of cellulose during reaction. This is an experimental challenge as cellulose cannot be quantified with traditional analytical techniques due to cellulose's poor solubility in water and other common organic solvents. Previous works studying cellulose activation use the change in sample mass during the experiment to probe the conversion of cellulose and model the kinetics of activation.[45,47] This approach is inadequate since solid char is produced during pyrolysis. During reaction, the measured mass will have contributions from the remaining reactant, char, and non-volatile intermediate chains; which causes underestimation of reactant conversion in these studies. To overcome this challenge, a kinetic surrogate for cellulose is required; where the surrogate molecule should exhibit similar chemistry to cellulose during pyrolysis and can be quantified easily with common analytical techniques. The first molecule intuitively to test as a possible surrogate for cellulose would be its monomer unit or glucose. However, glucose is not a suitable surrogate for cellulose since glucose is not produced during cellulose pyrolysis and glucose pyrolysis has a vastly different product distribution than cellulose pyrolysis.[19,83] Additionally, cellodextrins with a low degree of polymerization like cellobiose, cellotetraose, and cellohexaose are not suitable surrogates either as their product distributions also vary significantly from cellulose.

In contrast, cyclodextrins or cyclic oligosaccharides comprised of 6 (α), 7 (β), or 8 (γ) glucose monomers can be used as surrogate molecules for cellulose. Cyclodextrins have been previously shown to exhibit identical pyrolysis product distribution compared to

cellulose.[19,84] Zhu et al. also measured initial formation kinetics of various products from cellulose and α-cyclodextrin using the PHASR technique and observed all the products exhibited identical initial formation kinetics.[68] Since the overall product distributions and the initial product formation rates are identical, conversion of cyclodextrins and cellulose should also be kinetically similar. Lastly, cyclodextrins have high solubility in water, can be easily quantified using liquid chromatography, and satisfy both requirements to be a kinetic surrogate for cellulose. All subsequent work shown in this thesis measuring activation kinetics of cellulose will utilize α-cyclodextrin as a surrogate molecule for cellulose.

4.3: Experimental and Computational Methods

4.3.1: Preparation of Calcium Doped α-Cyclodextrin Thin-Film Samples

α-Cyclodextrin thin film samples were prepared via evaporative deposition on carbon steel heating elements. The heating elements were cleaned using a butane torch until they turned blue and afterwards were allowed to sit for 24 hours in ambient conditions. A 1.0 wt.% solution of α-cyclodextrin in HPLC water was prepared and the corresponding amount of $Ca(NO_3)_2 \cdot 4H_2O$ (0.1-0.5 mmol $Ca(NO_3)_2$/g α-CD) was added to the solution and thoroughly mixed to dope α-cyclodextrin with calcium. A 5.0 μL aliquot of the solution was pipetted onto the center of the cleaned heating element, corresponding to 50 μg of α-cyclodextrin. Samples were then placed under vacuum at 25 in. Hg and held at 40 °C until all the water had been evaporated and the film was completely formed. This deposition and drying technique was performed twice to generate 100 μg samples that were uniform circular films, <20 μm in thickness and 3mm in diameter.

4.3.2: PHASR Experiments

Reaction of α-cyclodextrin films were performed using the PHASR technique described in chapter 3. A prepared thin-film of α-cyclodextrin on the resistive heating element was inserted into the upper chamber of the PHASR reactor and then both chambers were sealed such that the copper electrodes contacted the resistive heating element. Inert helium sweep gas was then turned on and flowed through the upper chamber, over the sample and out of the reactor to prevent secondary reactions from affecting measured initiation kinetics. Thin-films were subjected to thermal pulses varying from 20 to 2000 milliseconds and temperatures between 370 and 430 °C. Once the thermal pulse was

applied to the sample, the resistive heating power supply turned off, and the sample was rapidly quenched via the high velocity Syltherm coolant.

4.3.3: Quantification of α-Cyclodextrin Conversion

Quantification of remaining α-cyclodextrin reactant after a pulse was performed via solvent extraction and liquid chromatography with light scattering detection. Heating elements containing partially reacted samples were removed from the PHASR reactor and cut into a small circle that only contained the sample film. The cut heating element was placed into a 1.5 mL PTFE filter vial. 350 μL of HPLC grade water was pipetted into each vial containing a heating element and vials were shaken for 1 minute to ensure complete dissolution of α-cyclodextrin. After complete dissolution, the remaining heating element was removed from the vial and the filter plunger was depressed to remove any remaining particulate. 100 μL of filtered sample was injected into a high-performance liquid chromatograph (HPLC, Shimadzu Prominence) with a carbohydrate separation column, (Agilent Na Hi-Plex, PN: 1171-6140) light scattering detector, (ELSD-LTII) and water mobile phase. Quantification of the α-cyclodextrin peak from the ELSD for PHASR pulses of increasing length yielded the consumption of reactant with time.

4.3.4: Computational Methods†

Calculations were performed using periodic plane-wave density functional theory which has been implemented using the Vienna Ab-initio Simulation Package (VASP).[85–87] The exchange and correlation energies were calculated using a form of generalized gradient

† The computational work in this chapter was performed by Vineet Maliekkal

approximation(GGA) functional developed by Perdew, Burke and Ernzerhof (PBE).[88] Most implementations of DFT fail to account for dispersion effects. To make up for this shortfall, the D2 method developed by Grimme, which can account for two-body interactions, was applied in all the calculations.[89,90] Plane waves were constructed using an energy cutoff of 396 eV along with projector augmented wave potentials (PAW) to model interactions between core and valence electrons.[91] A 1×1×1 k-points grid was found to be sufficient for the system based on energy convergence calculations.[92] The calculations were performed until self-consistent field calculations and geometric optimization converged to 10^{-6} eV & force of 0.05 eV/Å. The convergence criterion for force was considered optimal, because going to a tighter convergence criterion of 0.04 eV/Å changed the electronic energy only by around 2 kJ mol^{-1}, which is significantly lower than typical thermal energy (k_BT) of around 7 kJ mol^{-1}. To evaluate barriers for a mechanism, the climbing NEB method was used to generate intermediate images for the pathway and subsequently optimize the pathway with a force tolerance of 0.2 eV/Å.[93,94] The transition state was then obtained by using the highest energy images and the dimer method, as developed by the Henkelman group, with a force tolerance of 0.05 eV/Å.[95]

4.4: Kinetics of Calcium Catalyzed Activation

The conversion of α-cyclodextrin was measured for thermal pulses of 20-2000 milliseconds (ms), temperatures of 370-430 °C, and calcium concentrations of 0.1-0.5 mmol Ca^{2+}/g α-CD as depicted in Figure 4-1. Each data point is comprised of at least three independent experimental trials, and the error bars associated with each point represent a 95% confidence interval. From the data, it is evident that conversion of α-cyclodextrin exhibits apparent first order kinetic behavior with respect to α-cyclodextrin concentrations among all temperatures and calcium concentrations. For each temperature/concentration series, a first order kinetic model was fit to the experimental data and found to pass through a majority of the experimental confidence intervals. At 415 °C, pure α-cyclodextrin only achieved ~75% conversion after 2000 ms of reaction duration. In contrast, when α-cyclodextrin was doped with 0.5 mmol Ca^{2+}/g α-CD at 415 °C, a similar conversion was achieved within 100 ms and exceeded a conversion of 90% within 200 ms.

To characterize the effect of calcium catalyst, the experimental conversion data of Figure 4-1 were fit to a first-order kinetic model with apparent rate parameters, k_{app}, at each temperature and calcium concentration. The first order rate parameters were then plotted against the varying integer powers of calcium concentration. Figure 4-2 depicts this comparison for the data collected at 415 °C. It is evident that comparison with the square of calcium concentration exhibits the best linear fit and is the only integer power that successfully models the non-zero rate coefficient at zero calcium concentrations.[68] A similar trend is seen with the data collected at the other temperatures. Plots of the first order

rate parameters against the square of calcium concentration for all 6 temperatures is depicted in Figured 4-3.

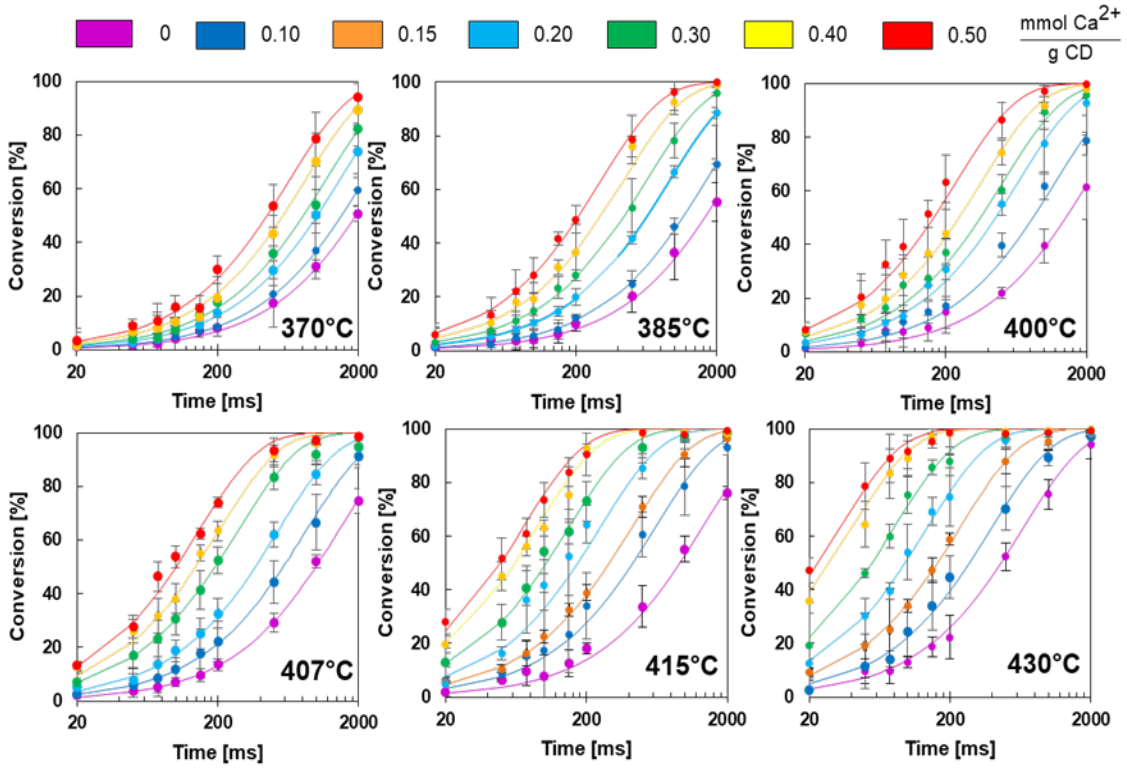

Figure 4-1. Kinetics of α-Cyclodextrin Conversion in the Presence of a Calcium Catalyst. Thermal activation of cyclodextrin was measured by determining conversion of cyclodextrin with varying loadings of Ca^{2+} catalyst (0-0.50 mmol Ca^{2+} g-CD^{-1}) and varying temperature (370 - 430 °C) with the PHASR technique. All experimental conditions exhibited first order kinetics in cyclodextrin conversion (●) fit to a first order model (-). Error bars represent 95% confidence intervals based on triplicate runs.

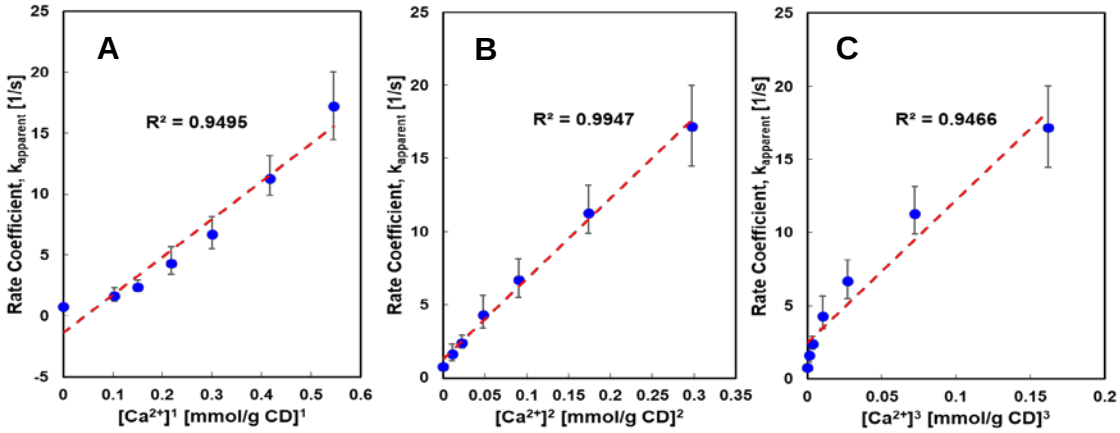

Figure 4-2. Comparison of First Order Rate Parameters Measured at 415 °C to Integer Powers of Calcium Concentration. (A) 1st, (B) 2nd, and (C) 3rd . The dashed red line represents the line of best fit for a simple linear regression and the coefficient of determination (R^2) is shown for each one. Comparison with calcium concentration squared gives the best linear fit. Similar behavior was seen with the 5 other temperatures. Error bars represent 95% confidence intervals.

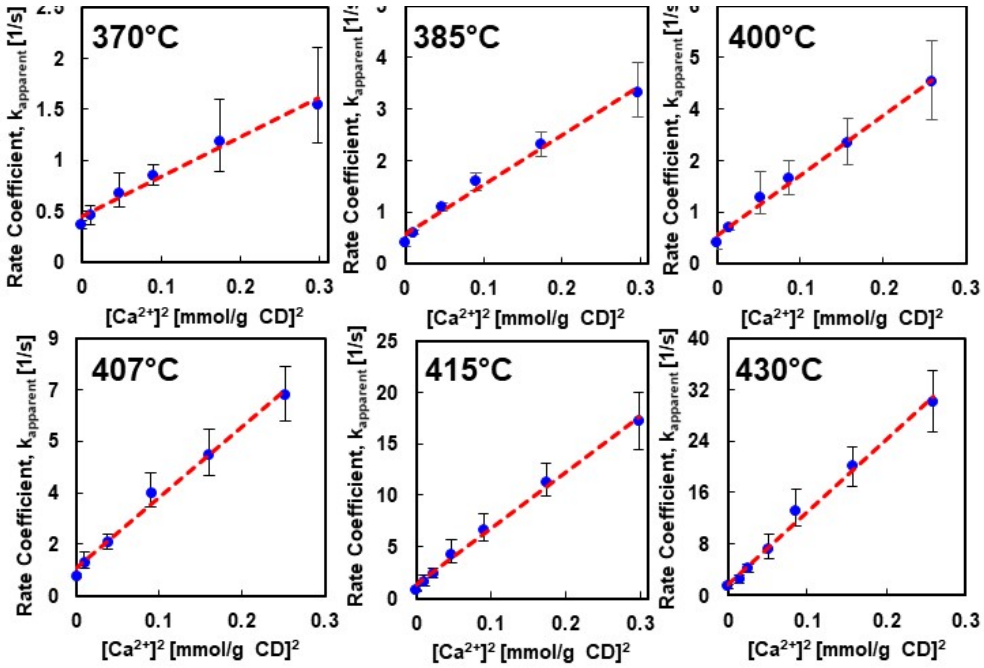

Figure 4-3. Comparison of First Order Rate Parameters to the Square of Calcium Concentration. Dashed Red lines represent line of best fit for a simple linear regression. Error bars represent 95% confidence interval.

From a mechanistic standpoint, this suggests a possible catalytic mechanism that proceeds through two calcium ions in the elementary steps. The rate of activation can simply be modeled as,

$$rate\ of\ reaction = (k_H + k_C[Ca^{2+}]^2) * M_{CD} \quad (4\text{-}1)$$

where k_H is a homogeneous or non-catalyzed rate constant, k_C is a catalyzed rate constant, and M_{CD} is the mass of α-cyclodextrin. This model was selected to incorporate the first order kinetic behavior with respect to α-cyclodextrin mass at all calcium concentrations, the second order dependence on calcium, and that the rate of reaction is non-zero when calcium is not present with the homogenous rate constant term. The catalyzed rate constant, k_C, can be extracted at each temperature by subtracting the total apparent rate constant by the known value of the homogenous rate constant at each temperature, before conducting a linear regression of these values versus the square of the calcium concentration. The catalyzed rate coefficients are presented in Arrhenius form in Figure 4-4. The first-order kinetic catalytic rate constant exhibits a high activation energy (E_a = 48.7 ± 2.8 kcal/mol) and a high pre-exponential factor ($k_0 = 1.28 \times 10^{17} \left(\frac{\text{mmol Ca}}{\text{g CD}}\right)^{-2} \cdot s^{-1}$).

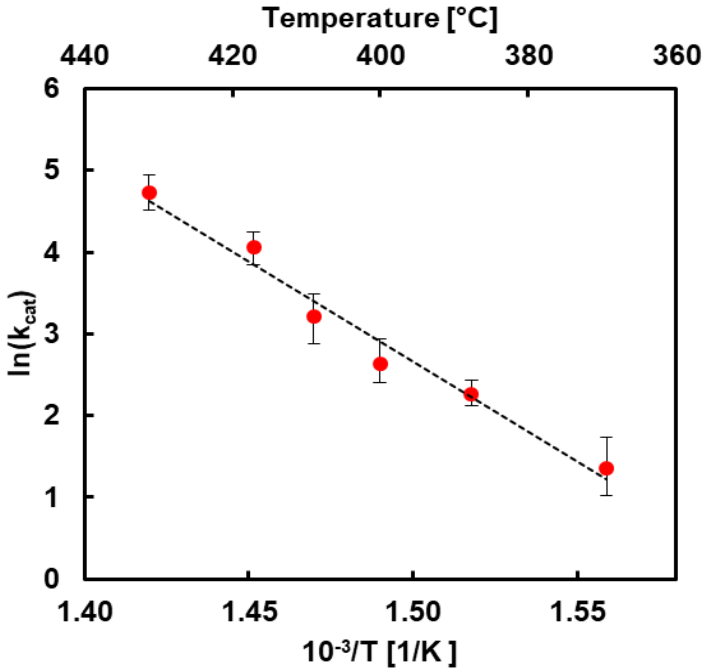

Figure 4-4. Calcium Catalyzed Activation Rate Constants Plotted in Arrhenius Form. Error bars represent 95% confidence interval.

Previous work utilizing PHASR studied activation of pure cellulose by measuring the conversion of α-cyclodextrin between 385-505 °C in the absence of any inorganic species.[68] The results indicate that activation exhibits two distinct kinetics regimes with a transition occurring at 467 °C, and exhibits a mechanism with high activation energy (~54 kcal/mol) and pre-exponential factor (~10^{16} s^{-1}) in the higher temperature regime. The similarity in value of activation energy of the metal-catalyzed rate constant and that of the non-catalyzed rate constant (~49 vs 54 kcal/mol) at higher temperatures motivated plotting of the total reaction rate constant (colored points) at different calcium concentrations along with the non-catalyzed rate constant (black points) on an Arrhenius plot, shown in Figure 4-5. The dashed color lines in Figure 4-5 represent a fit line for the rate constants by using

the expression for the total rate constant from equation 4-1 to combine contributions from the homogenous and catalyzed activation using the measured activation energies and Arrhenius pre-exponential factors from each. The data appear to fit a smooth curve as opposed to a plot with a sharp regime change such as with the non-catalyzed data points. A previous work proposed that this transition of kinetic regimes in neat cellulose is likely due to two underlying modes of activation – site specific, hydroxyl catalyzed transglycosylation which is dominant at lower temperatures and concerted thermal transglycosylation which is dominant at higher temperatures.[82] The lack of any such sharp transition in presence of calcium seems to indicate that the calcium catalyzed mechanism is unique and undergoes no such transition at similar temperatures. Also, it is evident that at increased calcium concentrations, catalyzed activation is significantly greater than non-catalyzed activation, further validating previous experimental results showing that the onset temperature is lowered in the presence of inorganic metals such as calcium.

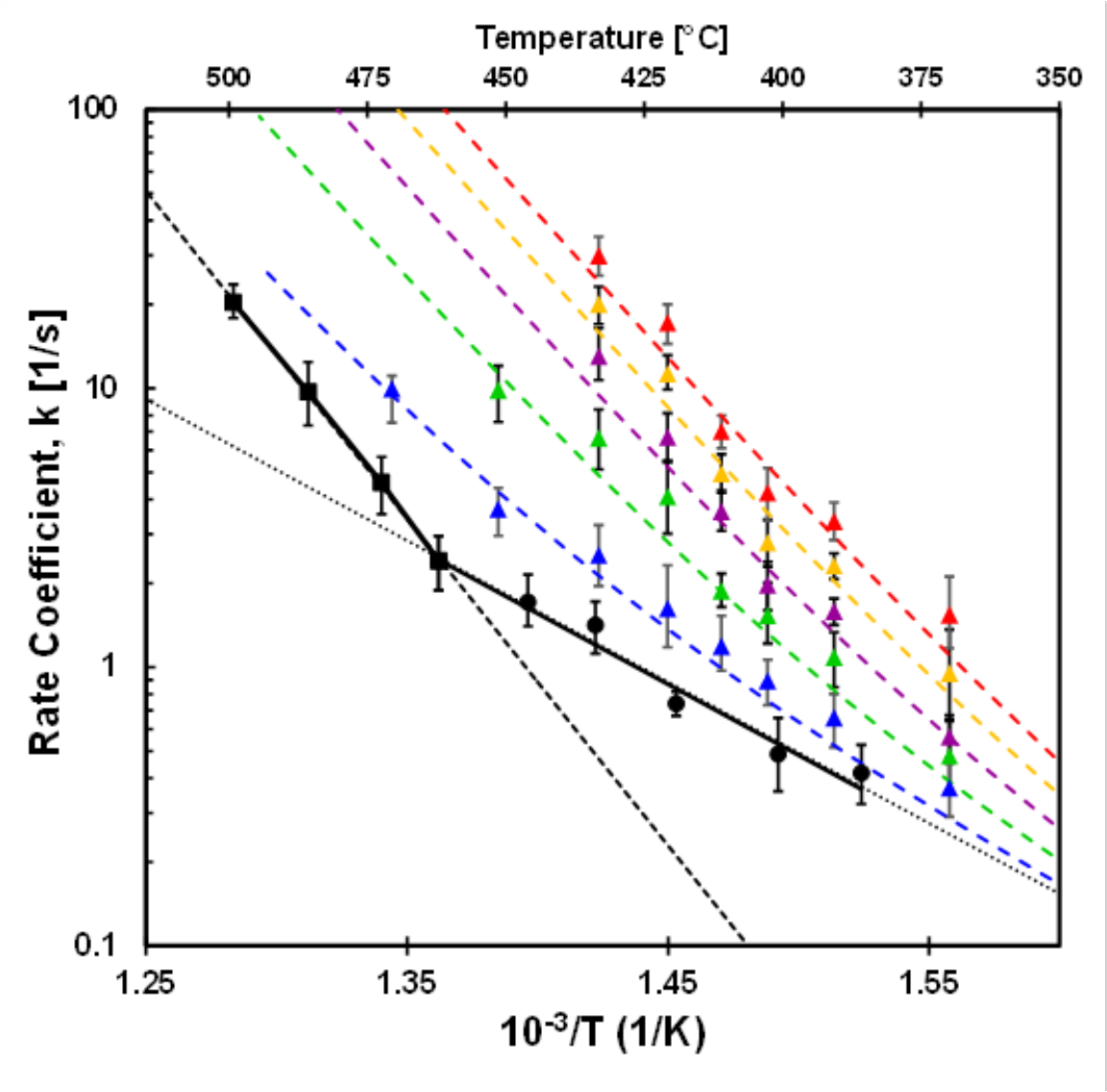

Figure 4-5. Global Interpretation of Calcium-Catalyzed Cellulose Activation. Arrhenius plot of uncatalyzed (black) and catalyzed cellulose activation (colored). Dashed color lines represent a fit for the activation rate constant with contributions from both catalyzed and noncatalyzed activation. Error bars represent 95% confidence intervals.

4.5: Investigating the Role of the Anion on Activation

All the experiments performed in this work incorporated various amounts of $Ca(NO_3)_2$ with the calcium cation assumed to be the catalyst for cellulose activation and the nitrate anion having negligible effects. While most studies also attribute the cationic species as the main catalyst, the anionic species has been shown to slightly alter pyrolysis product distributions.[55,57] Additionally, $Ca(NO_3)_2$ does not thermally decompose until 500 °C, so would be stable at the temperatures used in this work (370-430 °C).[96] Thus, it is important to investigate what effect the nitrate anion has on the kinetics of activation.

To test the effect of the counter anion, additional experiments with thin-films of α-cyclodextrin with $CaCl_2$ were performed. Time resolved conversion data of $CaCl_2$ doped α-cyclodextrin was obtained at three experimental conditions (0.3 and 0.5 mmol Ca^{2+}/g-CD at 400 °C and 0.5 mmol Ca^{2+}/g-CD at 430 °C) shown in Figure 4-6. The three test conditions were chosen to get appreciable catalytic reaction rates to easily discern if either anion has a significant effect on activation. Conversion of α-cyclodextrin still exhibits first-order kinetic behavior and first-order kinetic rate constants were extracted out. In all three conditions, the activation kinetics are similar between $Ca(NO_3)_2$ and $CaCl_2$ doped films with all the experimental points falling within experimental error, seeming to indicate the anion does not have significant effect on the kinetics.

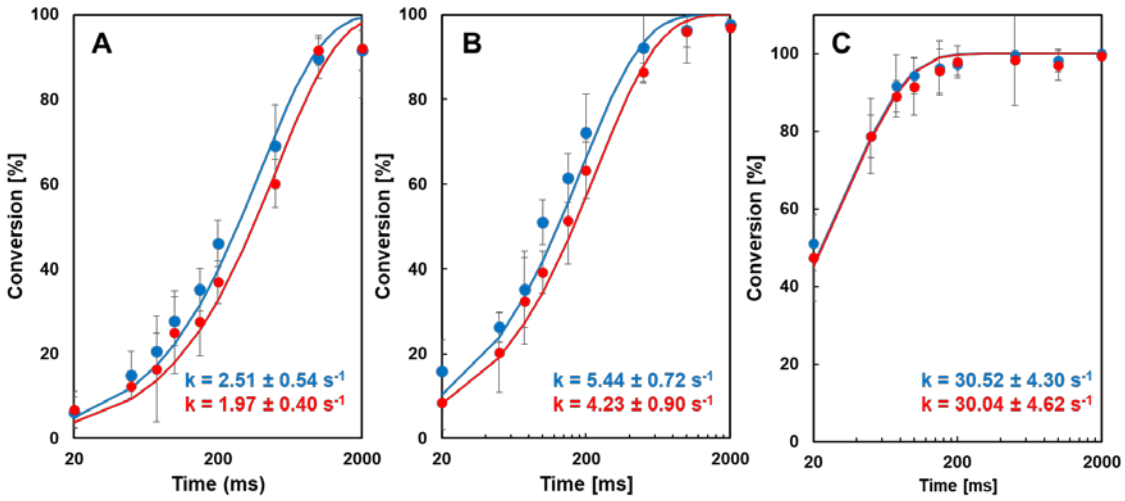

Figure 4-6. Time Resolved Conversion of α-Cyclodextrin with $Ca(NO_3)$ and $CaCl_2$ Salts at Three Different Conditions. (A) 0.3 mmol Ca^{2+}/g-CD at 400 °C. (B) 0.5 mmol Ca^{2+}/g-CD at 400 °C. (C) 0.5 mmol Ca^{2+}/g-CD at 430 °C. Blue points correspond to $CaCl_2$ doped films and red points correspond to $Ca(NO_3)_2$ doped films. Solid lines represent first-order kinetic fits. Error bars on points represent 95% confidence interval based on triplicate runs. Confidence interval for rate constants represent 95 % confidence intervals.

One hypothesis for this result can follow from the finding of a prior study by Jensen et al. looking at the effects of KCl on straw pyrolysis. In their findings, Jensen et al. report that 60% of the chloride ions are released as HCl between 200 and 400 °C.[97] It is then reasonable to hypothesize that the anions have little effect on activation kinetics because the anions extract protons from the hydroxyl groups in cellulose, form the corresponding acid and volatilize out of the cellulose melt at temperatures much lower than reaction.

To test this hypothesis, an online mass spectrometer (MKS Cirrus 2) was attached to the outlet of TGA (TA Instruments Q500) to analyze pyrolysis vapors of calcium salt doped cellulose and monitor if HCl or HNO_3, depending on whether cellulose is doped with $CaCl_2$ or $Ca(NO_3)_2$, evolves before reaction occurs. This experimental setup was used instead of

the PHASR technique, since PHASR is incapable of running experiments at temperatures lower than 250 °C and this experiment requires low temperature probing. To dope cellulose with calcium salts ($Ca(NO_3)_2$ and $CaCl_2$), 800mg of either $Ca(NO_3)_2 \cdot 4H_2O$ (>99% purity from Acros) or $CaCl_2$ (>96% purity from Sigma Aldrich) was dissolved in 20 mL of deionized water. 1g of microcrystalline cellulose (1g from Alfa Aesar, PN:A17730) was immersed in the calcium salt solution and stirred at room temperature for 2 hours. The ion-exchanged cellulose was collected by paper filtration and dried in an oven at 80 °C overnight to dry. The amount of calcium doped into the cellulose powder was confirmed using inductively coupled plasma optical emission spectroscopy, and both samples had a calcium concentration ~ 0.5 mmol Ca^{2+}/g-Cellulose. Additionally, a 1 molal nitric acid in silica powder was prepared to provide a rough calibration for spectrometer for the nitrate concentration initially present in the ion-exchanged samples.

During the experiment, about 5mg of sample was placed in a TGA pan and heated from 25 °C to 850 °C with a heating ramp of 20 °C/min, 100 mL/min of helium gas was flowed over the sample pan and the mass spectrometer monitored the intensities for m/z ratios of 36 and 46, the major peaks of HCl and HNO_3 respectively.[98,99] Figure 4-7 shows the intensity of these m/z ratios during the experiment for 5 different samples; an empty TGA cup (A), pure microcrystalline cellulose (B) silica with HNO_3 (C), $Ca(NO_3)_2$ exchanged cellulose (D), and $CaCl_2$ exchanged cellulose (E).

To dissect all the information presented in Figure 4-7, starting with an empty TGA pan (Figure 4-7A) no peak in the signal for HNO_3 or HCl is detected, indicating the pan itself does not attribute to any HNO_3 or HCl formation. The pan filled with 1 molal HNO_3 (Figure

4-7B) exhibits a peak in the HNO_3 signal at 4 minutes or when the set-point temperature is 105 °C which matches with the boiling point of HNO_3 at 81 °C. Additionally no peak in HCl signal is observed which is expected. The pan filled with pure microcrystalline cellulose (Figure 4-7C) exhibits no peak in the HCl signal but does exhibit a peak in the HNO_3 signal at 31 minutes or when the set-point temperature is 645 °C. This peak is attributed to some pyrolysis product, but this product was not identified. The pan filled with $Ca(NO_3)_2$ ion-exchanged cellulose (Figure 4-7D) also does not exhibit a peak in the HCl signal peak but does exhibits two peaks in the HNO_3 signal at 12 and 16 minutes corresponding to set-point temperatures of 265 and 325 °C respectively. Lastly for $CaCl_2$ ion-exchanged cellulose (Figure 4-7E), a peak for HCl formation is observed at 12 minutes and only 1 peak in the HNO_3 signal at 16 minutes is observed. Therefore, the peaks seen at 12 minutes in Figure 4-7 D and E are associated with the formation of the acids from the anions of the metal salts extracting protons from the cellulose matrix. HCl has a boiling point of 100 °C and should be volatile at the same point in these experiments as HNO_3 explaining why these peaks occur at the same time . The HNO_3 peak at 16 minutes for the metal doped samples is assumed to be a pyrolysis product catalyzed by calcium, but no identification of this compound was performed.

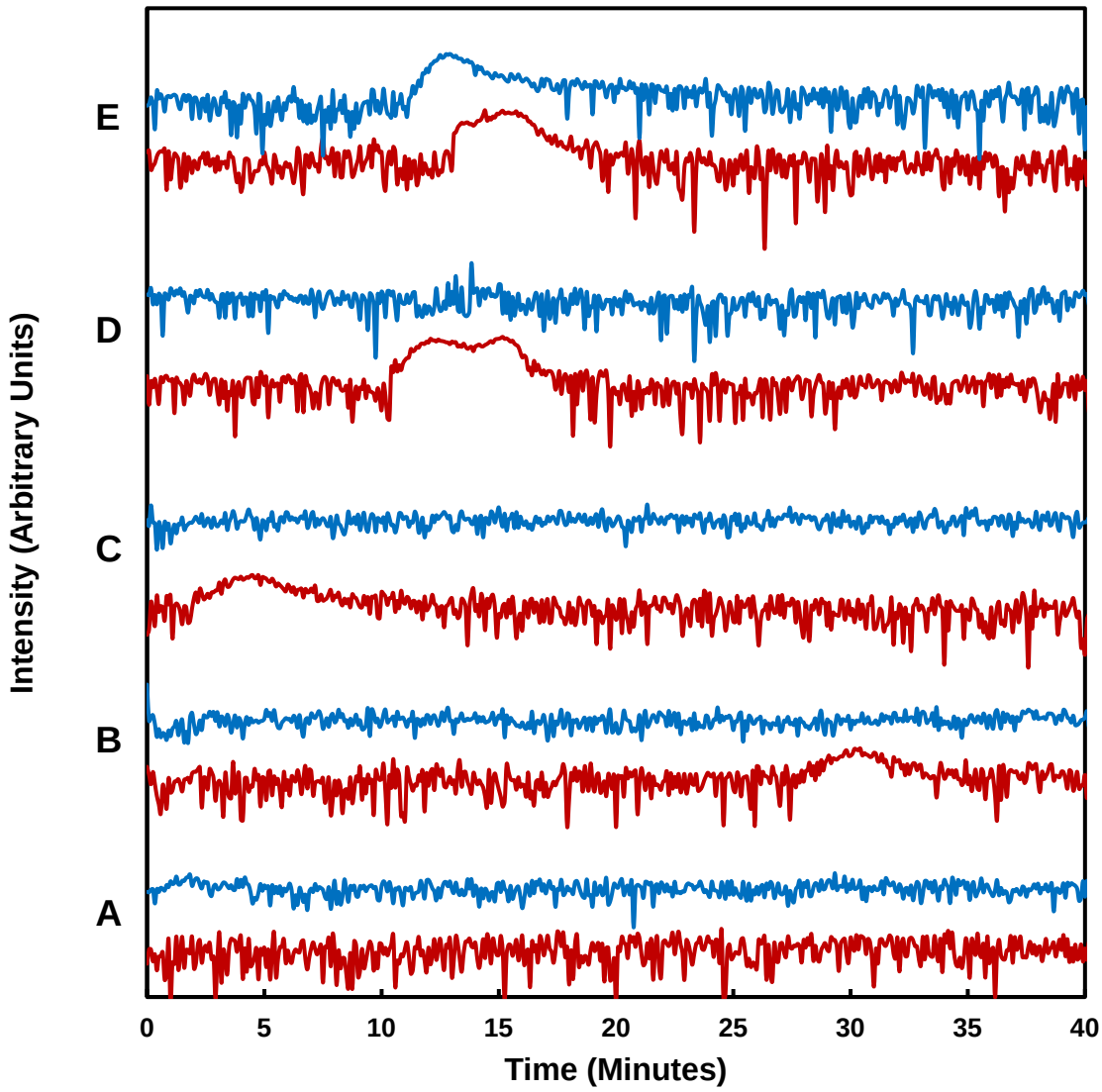

Figure 4-7. Online Mass Spectrometer Monitoring of HNO_3 and HCl Evolution of Calcium Doped Cellulose Samples. A) Empty pan. B) 1 molal HNO_3 in SiO_2 powder. C) Pure microcrystalline cellulose. D) $Ca(NO_3)_2$ doped cellulose. E) $CaCl_2$ doped cellulose. Blue line represents m/z of 36 corresponding to HCl. Red line represents m/z of 46 corresponding to HNO_3. Temperature ramp is 20 °C, with s tart temperature of 25 °C and final temperature of 850 °C. Pan filled with about 5mg of sample for each run.

The formation of HNO_3 and HCl with cellulose exchanged with $Ca(NO_3)_2$ and $CaCl_2$ seems to indicate that the anions do extract protons from the cellulose matrix and escape at temperatures much lower than the temperatures used for the PHASR experiments in this work (~265 vs 400 °C). Also, it is important to note that the set-point temperature within TGA can be much greater than the sample temperature during TGA, so the sample temperature that these peaks are observed at could be lower.[65] However, this set of experiments does not provide an answer for the rate at which the counterions extract the protons from cellulose during PHASR experiments. PHASR experiments occur with time scales on the order of milliseconds while these TGA experiments were with time scales on the order of minutes. Therefore, it is unknown how quickly the counterions are released during reaction and requires further testing to validate this.

4.6: The Nature of Active Sites and Interpretation of Kinetic Data

Before addressing the question of dominant catalytic mechanism, a deeper insight into the nature and structure of the active site is required. Previous studies suggest that metal ions can form chelated complexes with the hydroxyl groups of cellulose chains, and these could be active sites for catalysis.[100,101] Saddawi et al. in particular has suggested that metal ions prefer to form intra-molecular bridged sites between C_2-C_3 hydroxyl groups of a glucose monomer or between the C_6-C_3 hydroxyl groups of two adjacent glucose monomers.[102] While these hypothesized structures may be the stable binding sites at ambient conditions, the results from section 4.5 suggest that at reaction conditions the anions are releasing from the polymer melt as volatile acids. It can be then speculated that the hydroxyl groups of cellulose chains are likely providing protons for the anions to release as acids. In the absence of these protons, the deprotonated hydroxyl groups would likely be stabilized by calcium ions thus leading to a site comprising of Lewis acid, the calcium ion, and a Bronsted base, the deprotonated hydroxyl.

Subsequently, to scan for suitable locations in the cellulose matrix for such active sites to exist, a model was chosen which comprise of reacting sheet with degree of polymerization equal to 3 sandwiched in between two periodically extending cellulose sheets in an arrangement similar to the cellulose Iβ crystal (Figure 4-8A). The most stable binding site for calcium was found to be one where it sits as a bridging atom between the deprotonated states of C_6 and C_3 hydroxyl groups of two adjacent chains. This binding site was found to be more stable than any other binding site by 10-30 kJ/mol. As depicted by Figure 4-8, calcium binds strongly to the deprotonated hydroxyl groups which is evident

by the short Ca-O bond lengths of ~2.1 Å. Additionally, calcium forms weaker interactions, bond lengths between 2.3-2.9 Å, with up to 3 additional hydroxyl groups. Such Ca-O bond lengths are in excellent agreement with XRD studies of calcium impregnated carbohydrates.[103,104] Therefore, in all the DFT calculations discussed hereafter, this binding state of calcium is used as the resting state for the calcium catalyst. It must be noted that to carry out catalysis the calcium ion needs to be mobile and diffuse through the melt to bind to the reacting cellulose chain. To address the mechanism for calcium ion diffusion through the polymeric melt, a mechanism was first developed wherein hydroxyl groups in neighboring sheets could move to interact with these deprotonated sites and then subsequently transfer their protons to get deprotonated while grabbing the calcium ions themselves. This was verified by a simple model where two glucose monomers would interact with a typical calcium binding site and DFT calculations showed that this transfer mechanism has a low barrier ~ 3.5 kcal mol^{-1}. It is expected that such OH group interactions with calcium binding sites would be more prevalent in a melt phase as opposed to a solid phase since the oligosaccharides and light oxygenates produced in the melt during reaction would be able to interact and move around freely. Therefore, a periodic model was used that consisted of two cellulose sheets containing the impregnated calcium with oligosaccharides and water molecules being used to fill the space in between to signify trapped melting regions. Ab initio molecular dynamics simulations on these prototypical models for a semi-melt showed that the calcium ions can indeed move into the melt and bind themselves to sugars.

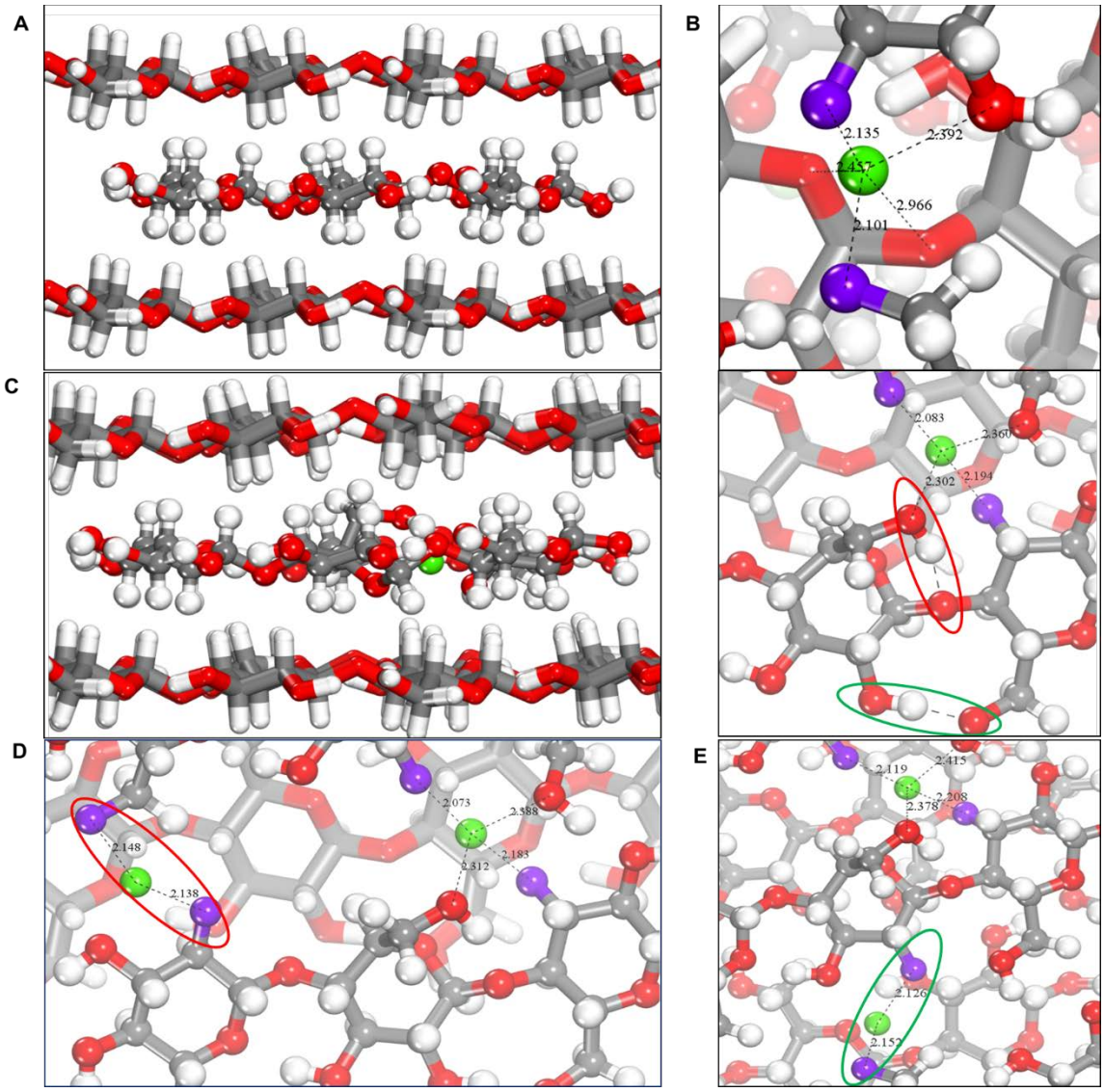

Figure 4-8. Molecular Structures of Neat and Calcium Incorporated Cellulose. (A) Model for neat reactant which consists of 2 extended sheets (shown in stick form) and a reacting sheet (shown in ball and stick form). (B) Optimized structure of most stable binding site for Ca. The active site consists of the metal ion, a Lewis acid site, and two deprotonated hydroxyl groups, a Bronsted base site (shown in purple). (C) Front view of bound reactant with a single Ca ion on the left and zoomed-in top view on the right. The hydroxymethyl group must rotate out of plane to form a hydrogen bond with the glycosidic O for reaction to occur (circled red). Breaking intra-molecular H-bonds(circled green) can improve reactivity. (D) In configuration 1, a second Ca ion is introduced to free up the hydroxymethyl group. (E) In configuration 2, a second Ca ion is introduced to disrupt intra-molecular H-Bond.

Having addressed the nature of the active site and the most stable binding position for calcium, the possible mechanisms for calcium catalyzed glycosidic activation are now discussed. The presence of rate order dependence calcium that is nearly second order suggests that two possible catalytic cycles could be in effect under pyrolytic conditions. Firstly, a catalytic cycle could be envisioned which involves the participation of a single calcium ion as shown below:

$$Ca + Cell \overset{K_1}{\Leftrightarrow} Ca\text{-}Cell$$

$$Ca\text{-}Cell \overset{k}{\rightarrow} Ca\text{-}Int$$

$$Ca\text{-}Int \overset{K_2}{\Leftrightarrow} Ca + Int$$

where *Cell* is the neat cellulose chain, *Int* is the post cleavage intermediate and *Ca* is the calcium catalyst. This would give a rate expression as follows:

$$rate = \frac{k * K_1 * [Cell][Ca]}{(1 + K_1[Cell])}$$

It is apparent that for such a cycle the measured rate order would be first order in calcium. Figure 4-8C shows one plausible candidate for the bound Ca-Cell intermediate wherein the calcium ion is closely interacting with the hydroxymethyl group and the glycosidic oxygen. In such a configuration, it is expected that calcium could catalyze the transglycosylation reaction, believed to be a dominant initiation mechanism, thus leading to a levoglucosan chain end intermediate.[53,82,105,106]

Looking closer at Figure 4-8C, it is evident that carrying out transglycosidic cleavage reactions in the presence of complex H-bonding networks could lead to energy penalties. For example, it is seen that the rotation of hydroxymethyl group, which is critical for transglycosylation, requires breaking multiple intra-sheet H-bonds and is likely to lead to an energy penalty. This energy penalty has been shown to increase the activation barriers

of transglycosylation from 51-53 kcal/mol in simple gas phase models to ~59 kcal/mol for such crystal models.[39] Similarly, there exist strong intra-molecular H-bonds that need to be stretched/broken during the course of reaction (circled in green in Figure 4-8C). It is possible for an additional calcium ion to bind in configurations such as those shown in Figure 4-8D and E respectively and thus disrupt such native H-Bonding networks that leads to potentially lower barriers. The two cases for double bonded calcium shown in Figure 4-8D and E are henceforth referred to as configuration 1 and 2 respectively. Therefore, in this scenario an alternative catalytic cycle can be proposed as follows:

$$Ca + Cell \overset{K_1}{\Leftrightarrow} Ca\text{-}Cell$$

$$Ca + Ca\text{-}Cell \overset{K_2}{\Leftrightarrow} Ca\text{-}Cell\text{-}Ca$$

$$Ca\text{-}Cell\text{-}Ca \overset{k}{\rightarrow} Ca\text{-}Int\text{-}Ca$$

$$Ca\text{-}Int\text{-}Ca \overset{K_3}{\Leftrightarrow} Ca + Ca\text{-}Int$$

$$Ca\text{-}Int \overset{K_4}{\Leftrightarrow} Ca + Int$$

which gives a rate expression that looks as follows:

$$rate = \frac{k * K_1 * K_2 * [Cell][Ca]^2}{(1 + K_1[Cell] + K_1 * K_2[Cell][Ca])}$$

For such a catalytic cycle, it becomes clear that second order rate dependence of calcium in the rate of activation could be possible. While it is likely that the second catalytic cycle would have a lower activation barrier the concentration species such as Ca-Cell-Ca may also be much lower than Ca-Cell. Therefore, it is possible to observe rate orders between 1 to 2 in calcium depending on the range of calcium concentration experiments are operated in. In the next section, a detailed discussion of the DFT calculated energetics is presented to compare the two catalytic cycles.

4.7: DFT Calculated Energetics for Calcium Catalytic Cycles

Reaction energy profiles for activation using either a single calcium ion or two calcium ions are depicted in Figure 4-9 and 4-10. Figure 4-11 depicts the optimized transition states for each of the cases in Figure 4-9 and 4-10. Considering first the energetics of the single calcium catalytic cycle in Figure 4-9, it is seen that the bound reactant in the boat conformer (necessary to carry out transglycosylation) is 17.2 kcal/mol uphill in energy. This uphill energetic penalty is likely due to two reasons – (1) a penalty is paid to move the calcium ion from its most favorable binding site to the site where it carries out catalysis (2) a penalty is paid to break intra-sheet H-Bonds for rotating the hydroxymethyl group. The calculated activation barrier is 52.7 kcal/mol which is lower than the barrier for carrying out transglycosylation in a neat cellulose crystal (~59 kcal/mol). This leads to the speculation that one of the primary roles of calcium in this chemistry is to stabilize charged transition states due to its Lewis acidic nature. This is visible in the optimized transition state structure in Figure 4-11A, where the calcium ion forms a strong bonding interaction (Ca-O bond length 2.29 Å) with the negatively charged hydroxymethyl oxygen. From the energetics of this cycle one can thus expect to observe rate orders equal to 1 and barriers that are a little higher than those observed in experiments (~49 kcal/mol).

Moving on to the catalytic cycle when using two calcium ions in configuration 1 (Figure 4-10A), it is evident that while an energetic penalty is paid to move in the first calcium ion, the introduction of a second calcium ion leads to a very stable chair conformer double calcium bound reactant that is 6.8 kcal/mol downhill in energy. The reason for this very stable conformation is that the second calcium ion, as mentioned previously, is used

to free up the hydroxymethyl group. This allows the hydroxymethyl group to rotate and form a highly stable chair conformer where it interacts to form a strong bond with the primary catalytic calcium ion near the reaction center. In this scenario, an intrinsic barrier of 47.6 kcal/mol and an apparent barrier of 40.8 kcal/mol is observed, which is much lower than the barriers calculated for the single calcium catalytic cycle. This is a possible indication of the secondary role that calcium could play by freeing up critical hydroxymethyl groups. This is supported by the geometry of the optimized transition state in Figure 4-11 which is nearly identical to that observed for the single calcium case thus indicating that the additional calcium ion only plays a secondary role.

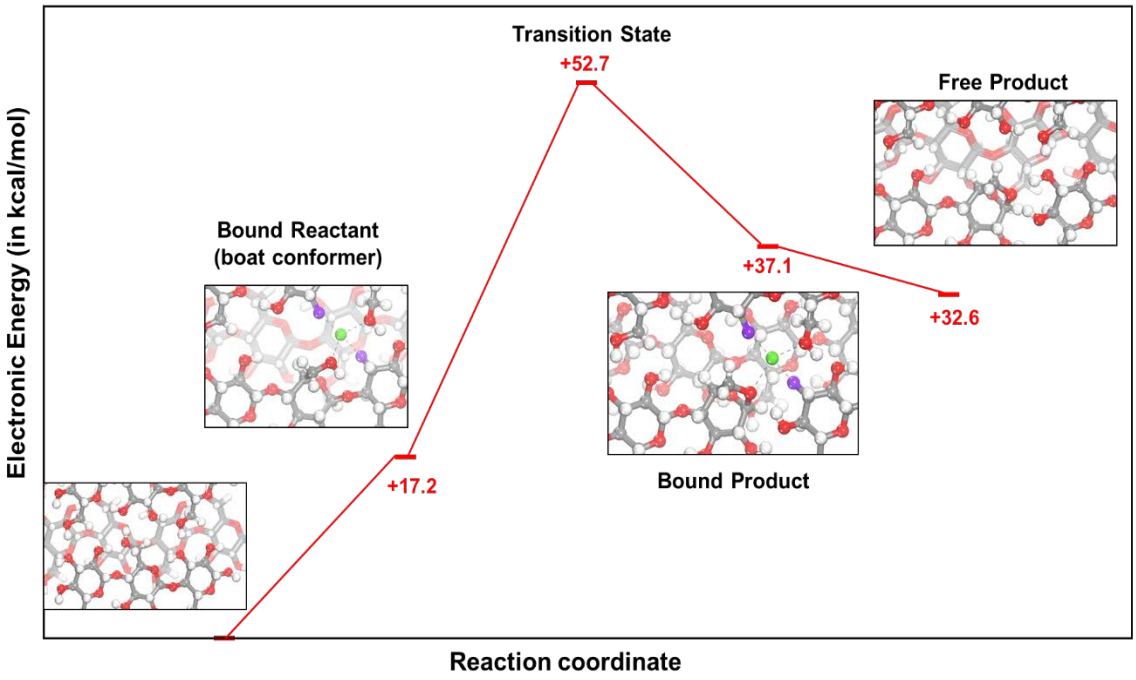

Figure 4-9. Reaction Energy Profile for Ca-Catalyzed Reaction in the Single Calcium Ion Case.

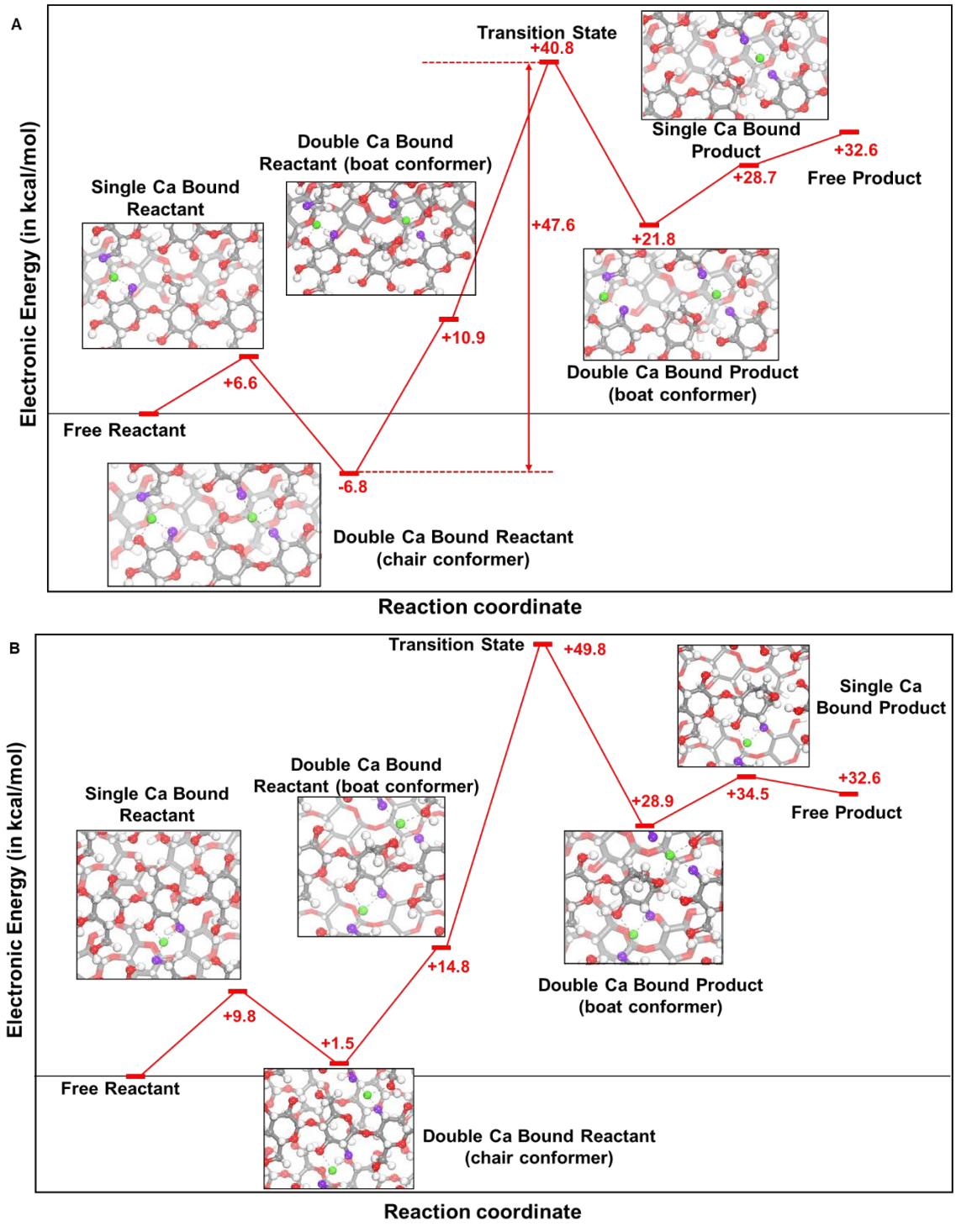

Figure 4-10. Reaction Energy profile for Ca-catalyzed reaction when two calcium ions are considered in either (A) configuration or (B) configuration 2.

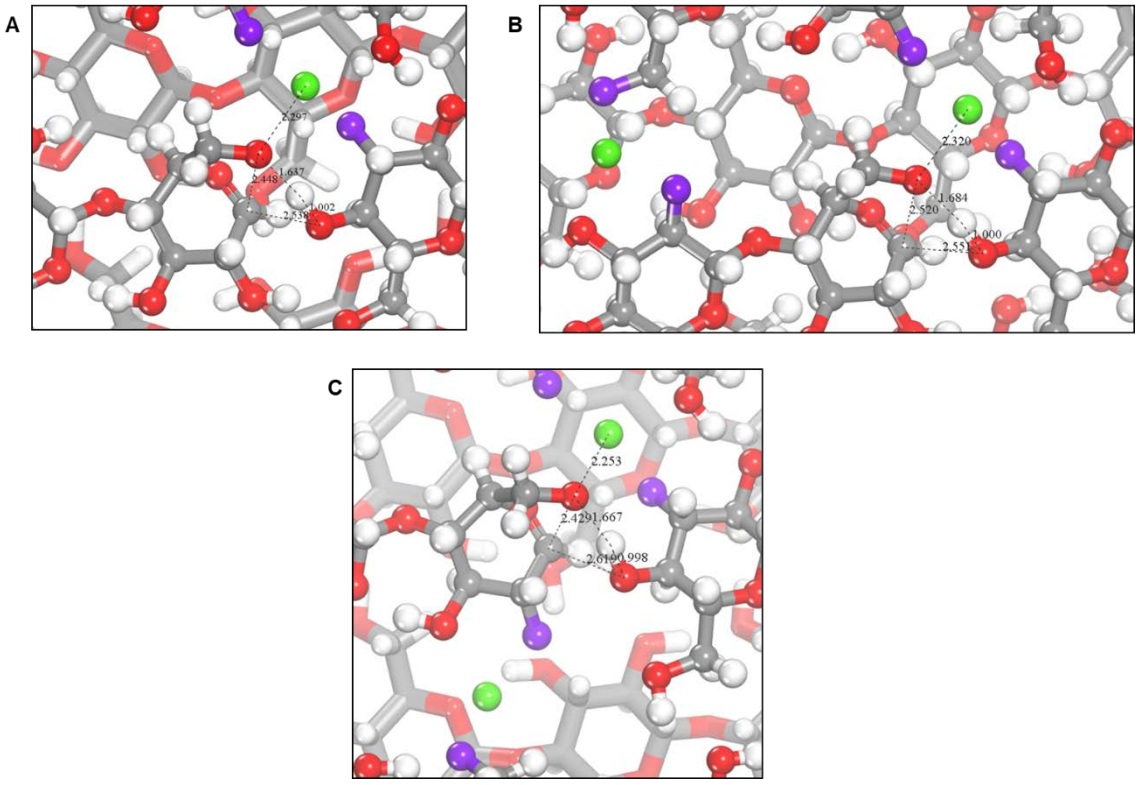

Figure 4-11. Optimized Transition State Structures. (A) Single Ca case (B) configuration 1 with two Ca ions (C) configuration 2 with two Ca ions.

Finally, in configuration 2 (Figure 4-10B), it is seen that the double calcium bound boat conformer reactant is 14.8 kcal/mol uphill in energy vs 17.2 kcal/mol in the single calcium case. This is because as highlighted in Figure 4-8E, the second calcium ion breaks a strong intramolecular H-bond, and this facilitates not just conformational changes but also facile cleavage of the glycosidic bond. This is visible in the calculated activation barrier which is about 3 kcal/mol lower than the calculated barrier for the single calcium case (49.8 vs 52.7 kcal/mol). This calculated barrier is also in excellent agreement with the experimentally measured barrier.

Thus, through configurations 1 and 2 it is shown that catalytic cycles can be envisioned with two calcium ions participating in them. Accordingly, switching from very low to high concentrations of the calcium salt should lead to observed rate order changing from 1 to 2. The concentration range chosen for experiments in this work is between 0.1 to 0.5 mmol/g cyclodextrin which is representative of real biomass salt concentrations but is likely too small a range (less than an order of magnitude) to observe these hypothesized changes in rate orders. It must also be noted that in the presence of salts, non-integer rate orders can also be the result of treating concentrations and activities to be the same.[107] However, in absence of a reliable model or experimental technique to calculate or measure activity coefficients for such polymer melts it is difficult to make any claims regarding this.

4.8: Conclusions

Combining the novel PHASR reactor with first principle density functional theory calculations, a fundamental chemical mechanism for calcium catalyzed activation of cellulose is elucidated. Temporally resolved conversion data of α-cyclodextrin reveals a dramatic acceleration of cellulose activation in the presence of calcium. Experiments also reveal that cellulose activation exhibits second order rate dependence on calcium concentration. DFT calculations, through the use of explicit cellulose crystal models, suggest that the second order behavior may be attributed to calcium playing a strong, primary catalytic role of stabilizing charged transition states while also playing secondary roles of disrupting the native H-bonding networks and, hence enhancing reactivity. Additional studies are required to completely describe the effect of calcium on the complete reaction network during thermochemical conversion of biomass. Additionally, the effect of other naturally present metals such as potassium and magnesium will have to be examined to discern fundamental mechanistic differences between metals in this complex reaction sequence.

Chapter 5: Magnesium Assisted Activation of Cellulose

5.1: Introduction

While chapter 4 thoroughly elucidates the catalytic role of calcium in thermal activation of cellulose, additional studies detailing the role of the other inorganic material naturally present in biomass on this chemistry are required. The behavior of the other alkali and alkaline earth metals (Na^+, K^+, and Mg^{2+}) on this chemistry is of particular interest as they exist in comparable amounts to calcium in biomass and are commonly seen as the most catalytic species.[24,57] Additional studies should look to describe how the properties of metal cations, especially the size and oxidation state of the cation, affect activation chemistry. Insight into the role these cationic properties have on activation chemistry can then be easily applied to chemical models detailing the catalytic effect of alkali and alkaline earth metals on individual product formation. In addition to the intuitive need for further investigation on the other alkali and alkaline earth metals, knowledge of metal cationic properties can be applied to experiments and models studying the various other metals in biomass (iron, zinc, copper, nickel, etc.) that exist in a wide range of cationic sizes and oxidation states.[108]

The mechanism for calcium catalyzed activation presented in chapter four describes the calcium cation playing two catalytic roles in the chemistry; disrupting the hydrogen bonding network to allow facile rotation of the C_6-hydroxymethyl group for transglycosylation and electronically stabilizing the charged transition state. Since assisted transglycosylation has been shown to a preferred mechanism for glycosidic bond cleavage, this mechanism should be extendable to other cations.[39,53,82] The extent these two catalytic roles are utilized for other metals should be linked to the size and oxidation state of the

cation. The extent of disruption of the hydrogen bonding network, is characterized by the number of deprotonated hydroxyl groups the cation binds to and the ability for the cation to fit in between two chains of cellulose. This is dependent on both the size and oxidation state of the cation ion. Stabilization of the transition state was due to the Lewis acidic nature of the metal cation. Lewis acidity is also correlated to both the size and oxidation state of the cation. Following conventional periodic trends, as one moves along a period, the size of the cation decreases, which increases the electron ionization energy and thus increases the ion's Lewis acidity.[109] This would be the case when comparing potassium to calcium. Additionally when moving down a group, the size of the cation increases and the Lewis acidic characteristic decreases; the case when comparing magnesium to calcium. Differences in the kinetics based on changes in ionic size or oxidation state should be evident when comparing calcium catalyzed activation to either potassium or magnesium catalyzed activation. For calcium versus magnesium (Ca^{2+} vs. Mg^{2+}), this should detail the effect of ionic size. In the case of calcium compared to potassium (Ca^{2+} vs. K^{+}), this should detail the effect of the oxidation state.

In this chapter, time-resolved kinetic data for magnesium catalyzed activation are presented and the results are compared to the ones presented in chapter 4. To allow for direct comparison with calcium, the kinetics were measured following identical experimental methods to those used in chapter 4, with the only exception being magnesium was incorporated into α-cyclodextrin by adding $Mg(NO_3)_2 \cdot 6H_2O$ to the 1 wt.% solution of α-cyclodextrin in water. Otherwise, procedures for thin-film preparation, PHASR runs, and analytical quantification were identical to those detailed in section 4.3. Additionally, no computation work to supplement the experimental kinetics was conducted at this point in time.

5.2: Kinetics of Magnesium Catalyzed Activation

The conversion of α-cyclodextrin was measured for thermal pulses of 20-2000 milliseconds (ms), temperatures of 370-430 °C, and magnesium concentrations of 0.1-0.5 mmol Mg^{2+}/g α-CD as depicted in Figure 5-1. Each data point is comprised of at least three independent experimental trials, and the error bars associated with each point represent a 95% confidence interval. Similar to calcium case, conversion of α-cyclodextrin exhibits apparent first order kinetic behavior with respect to α-cyclodextrin concentrations among all temperatures and magnesium concentrations. For each temperature/concentration series, a first order kinetic model was fit to the experimental data and found to pass through a majority of the experimental confidence intervals. The presence of magnesium also significantly accelerates the rate of α-cyclodextrin with rates comparable to those seen in the calcium data.

Following a similar though process, the experimental conversion data of Figure 5-1 were fit to a first-order kinetic model with apparent rate parameters, k_{app}, at each temperature and calcium concentration and were plotted against the varying integer powers of calcium concentration. Comparable to calcium, the first operate rate parameters follow a linear fit with the square of magnesium concentration at all temperature and this is depicted in Figure 5-2.

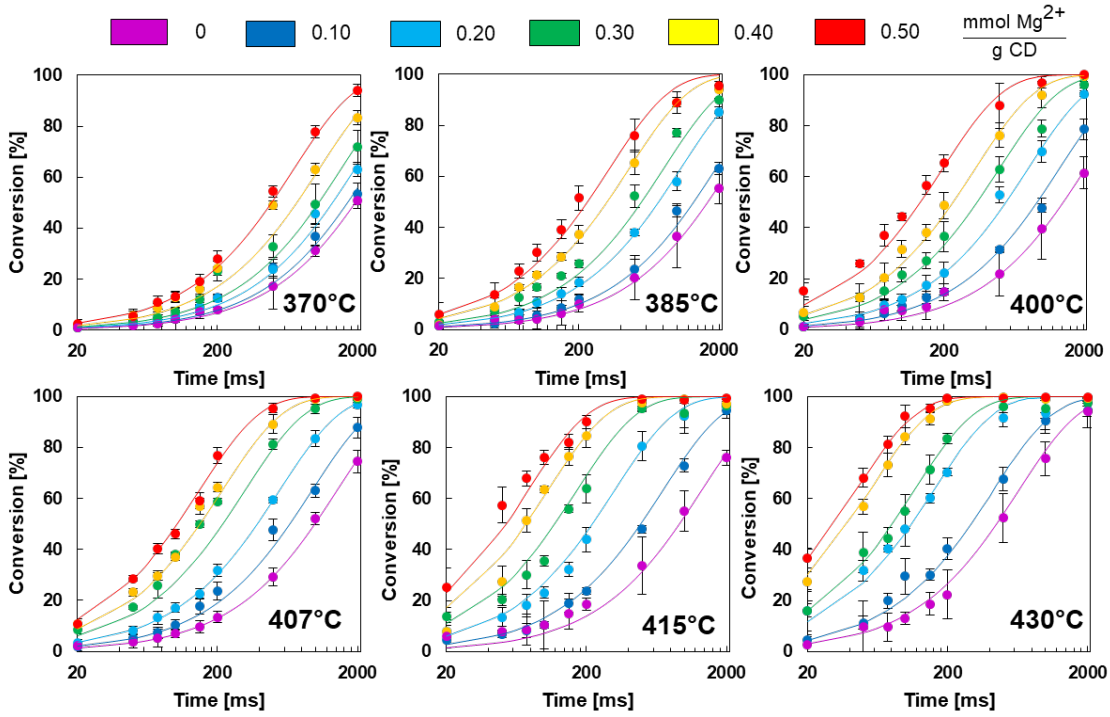

Figure 5-1. Kinetics of α-Cyclodextrin Conversion with Magnesium Catalyst. Thermal activation of cyclodextrin was measured by determining conversion of cyclodextrin with varying loadings of Mg^{2+} catalyst (0-0.50 mmol Mg^{2+} g-CD^{-1}) and varying temperature (370 - 430 °C) with the PHASR technique. All experimental conditions exhibited first order kinetics in cyclodextrin conversion (●) fit to a first order model (-). Error bars represent 95% confidence intervals based on triplicate runs.

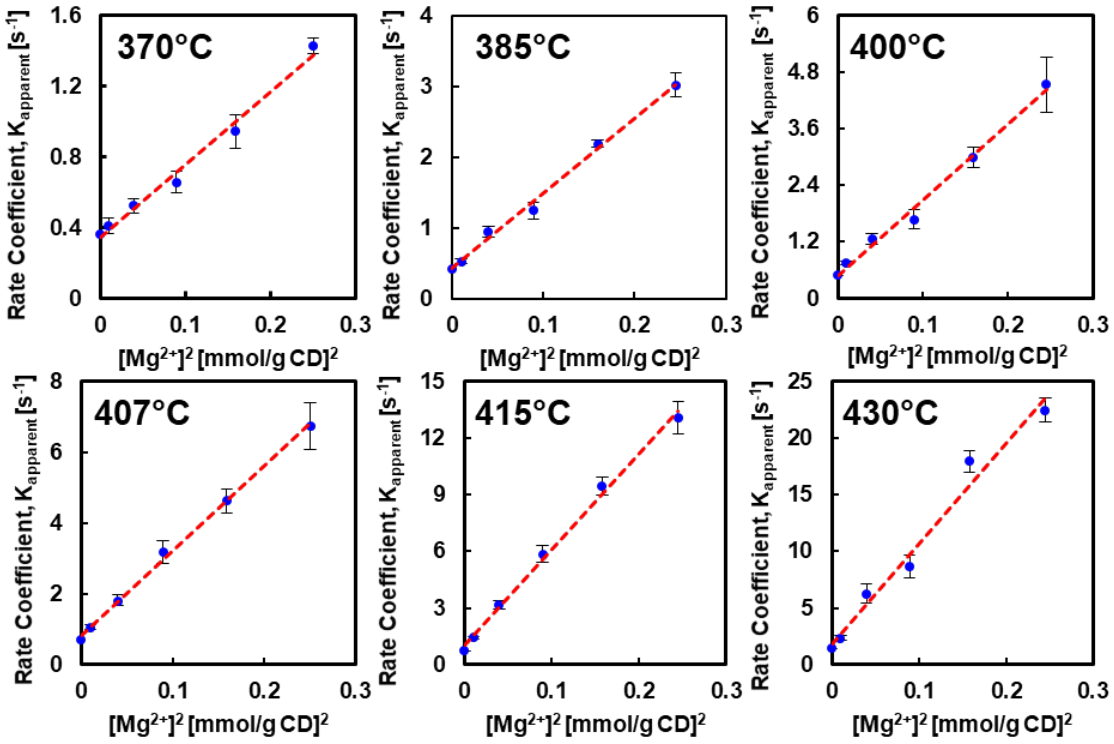

Figure 5-2. Comparison of First Order Rate Parameters to the Square of Magnesium Concentration. Dashed Red lines represent line of best fit for a simple linear regression. Error bars represent 95% confidence interval.

With α-cyclodextrin conversion still exhibiting first order conversion behavior in α-cyclodextrin concentration and second order dependence of magnesium concentration a rate expression similar to equation 4-1 is constructed,

$$rate\ of\ reaction = (k_H + k_C[Mg^{2+}]^2) * M_{CD} \qquad (5\text{-}1)$$

where k_H is a homogeneous or non-catalyzed rate constant, k_C is a the magnesium catalyzed rate constant, and M_{CD} is the mass of α-cyclodextrin. In a similar fashion, the catalyzed rate constant, k_C, can be extracted at each temperature by subtracting the total apparent rate

constant by the known value of the homogenous rate constant at each temperature, before conducting a linear regression of these values versus the square of the magnesium concentration. The catalyzed rate coefficients are presented in Arrhenius form in Figure 5-

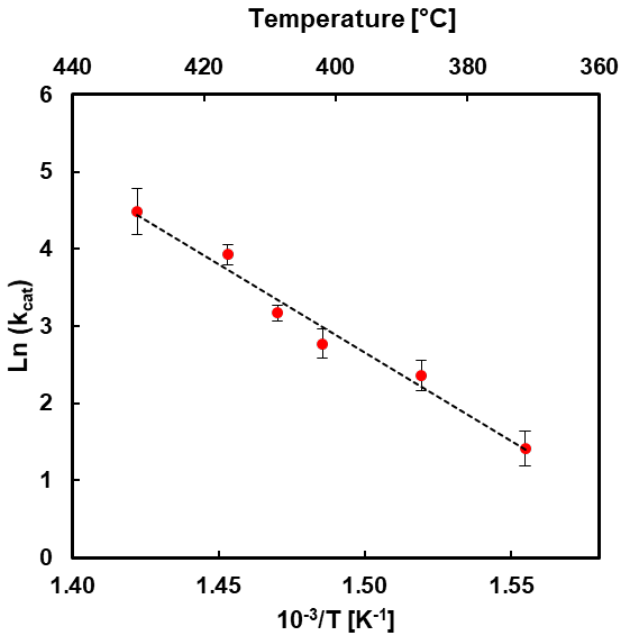

Figure 5-3. Magnesium Catalyzed Rate Constants Plotted in Arrhenius Form. Error bars represent 95% confidence interval.

3. The first-order kinetic catalytic rate constant exhibits an activation energy of 45.6 ± 2.1 kcal/mol) and a pre-exponential factor of 1.18 x 10^{16} $(\frac{\text{mmol Mg}}{\text{g CD}})^{-2} \cdot s^{-1}$.

A previous crystallographic study measured the ionic radii of magnesium and calcium ions which are 0.72 and 1.0 Å respectively.[110] The measured Arrhenius parameters for magnesium catalysis seem to follow with conventional periodic trends related to ionic size. The smaller magnesium ion has a greater Lewis acidity and thus would provide greater stabilization of the transition state and decrease the activation energy ($E_{a,Mg}$ = 45.6 kcal/mol vs $E_{a,Ca}$ = 48.7 kcal/mol). The pre-exponential factor has been associated with the number

of available sites along the cellulose chain that transglycosylation can be performed.[68,82] From this, it appears the smaller magnesium ion seems to disrupt the hydrogen bonding network to a lesser degree than calcium and is reflected in the pre-exponential factor being an order of magnitude smaller (~10^{16} vs 10^{17}).

While the energetics seem to follow period trends, there is not a great difference in these values especially when the confidence intervals of these values are taken into account, making it difficult to truly attribute at differences in kinetics due to a reduction in ionic size. This small difference can be noticed further when a parity plot of the total apparent rate constants from the magnesium and calcium catalyzed data is constructed, shown in Figured 5-4. Each point in the plot compares the rate constant obtained at identical metal concentration and reaction temperature. From Figure 5-4 it is evident that almost all the points, except for a few points measured under high temperature and high metal concentration in the upper right of the plot, fall along the one to one trend indicating the apparent rate constants appear to be identical between the two metals. To further question if the energetics are different, a statistical hypothesis test comparing the measured catalytic activation energies was performed.[111] In the hypothesis test, the null hypothesis was chosen so the two activation energies are assumed to be identical and would have to show with statistical significance, or the probability value is much smaller than some acceptable significance level(~ 0.05), they are different to reject this claim. From this hypothesis test, the obtained probability value is 0.646 and since it is much greater than any acceptable significance level, it cannot be claimed that there is a statistical difference in the energetics of catalyzed activation in the presence of magnesium and calcium.

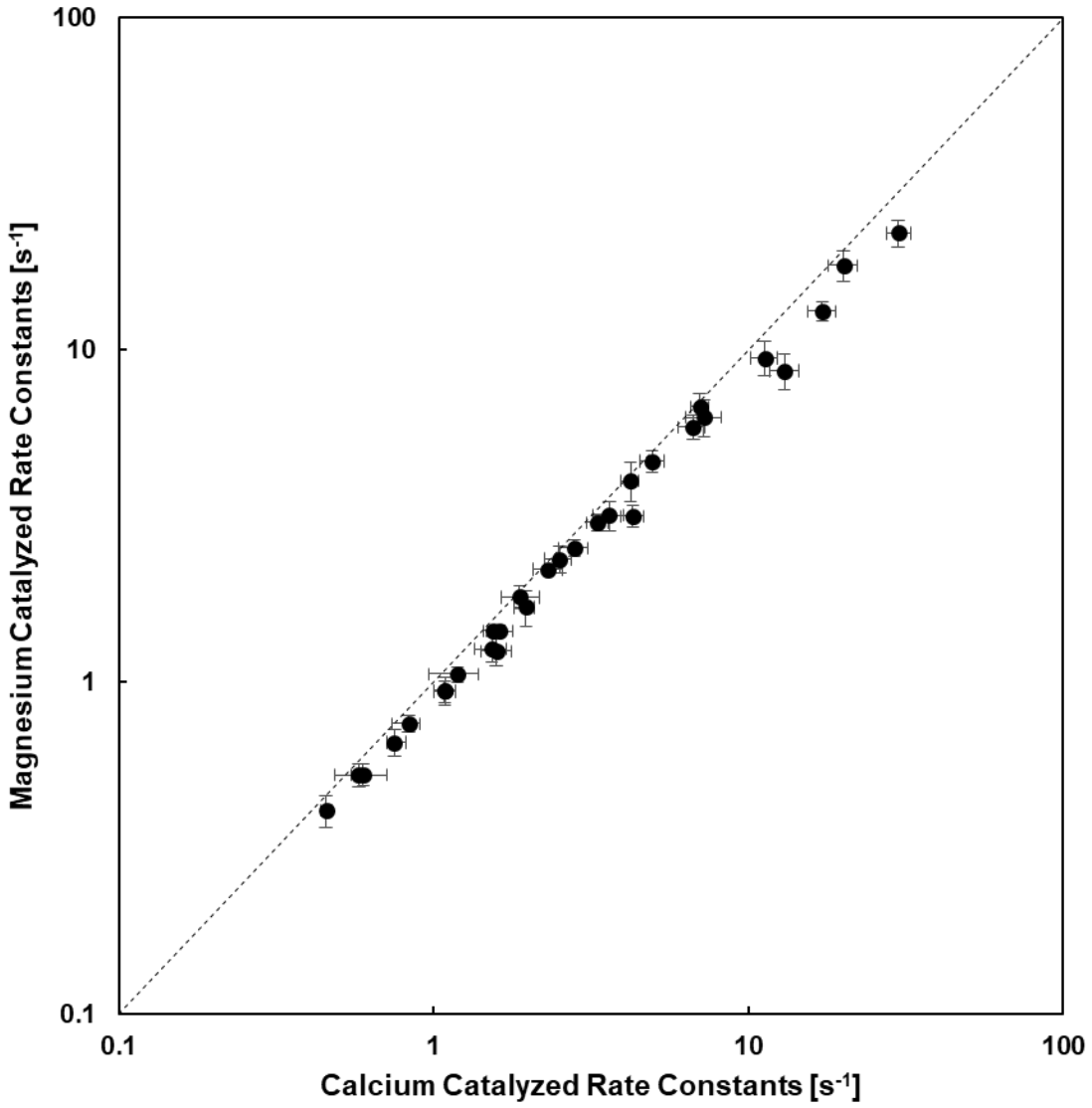

Figure 5-4. Comparison of Total Apparent Rate Constants for Activation in the Presence of Magnesium or Calcium. Points correspond to rate constants measured at identical metal concentration and reaction temperature. Dashed line represents one to one trend line. Error bars represent 95% confidence intervals.

At the time this chapter was written, no computational work is available to explain this result. However, the mechanism for catalyzed activation presented in chapter 4 and the configuration of cellulose can provide some insight. First, the distance between two chains of cellulose and the ionic radius of magnesium and calcium should be considered. Cellulose Iβ, the crystal structure of cellulose used in the simulation for chapter 4, has cellulose chains within one sheet separated by about 1.5 Å.[112] The ionic radii of magnesium and calcium are 0.72 and 1.0 Å respectively.[110] So magnesium and calcium ions should fit between two chains of cellulose without limitation and possibly disrupt the hydrogen bonding network to the same degree, which would produce equivalent pre-exponential factors. Additionally, DFT calculations where only 1 calcium ion participates in the reaction (Figure 4-9) indicate that presence of calcium to stabilize the transition state provides about 7 kcal/mol energetic benefit as compared to the neat case (~52 vs 59 kcal/mol), which is not a significant difference in energy. It is possible that the difference in Lewis acidity between magnesium and calcium is not great enough to be measured by these kinetic experiments.

Moving forward, it is necessary to perform DFT calculations to determine if magnesium promotes activation in an identical fashion mechanistically compared to calcium. Insight into the specific locations magnesium interacts with the cellulose matrix will enable proper analysis to determine if differences in ionic radii have an effect on the chemistry. An additional set of experiments that could be useful is to study the effect that larger alkaline earth metals, such as barium, have on this chemistry. While these metals are not present in lignocellulosic feedstocks, they have ionic radii large enough to possibly discern differences. Barium has an ionic radius of 1.49 Å, or almost identical to the distance

between two chains of cellulose.[110] Barium could then disrupt the hydrogen bonding to a much different extent than calcium or magnesium. The greater ionic radius of barium could also allow for discerning differences based on the Lewis acidity of the ion too.

Chapter 6: Conclusions

Biomass fast pyrolysis has considerable potential for the production of renewable fuels and chemicals. Despite decades of fundamental studies, there is no complete description of pyrolysis chemistry. In particular, mechanisms detailing how the polymer chains of cellulose initial fragment and the main reaction pathways towards the other major products are heavily debated. Additionally, inorganic metals naturally present in biomass such as alkali and alkaline earth metals have been known to alter pyrolysis chemistry drastically but their role in the mechanisms of pyrolysis chemistry is even less understood. This lack of knowledge into pyrolysis chemistry can be directly attributed to the inability to measure intrinsic kinetics of this process.

In this thesis, an experimental reactor capable of measuring kinetics of biomass pyrolysis, PHASR, is presented. 5 requirements for measuring pyrolysis kinetics are discussed and PHASR is shown to be capable of satisfying these requirements unlike other commonly used reactors utilized in pyrolysis studies.

The PHASR technique was then used to study calcium assisted activation of cellulose. Temporally resolved kinetic measurements of calcium doped α-cyclodextrin thin films demonstrated calcium rapidly accelerates the rate of glycosidic bond cleavage at lower temperatures than in non-catalyzed activation. DFT computations were used to unveil that calcium acts with two catalytic roles in thermal activation; disruption of the hydrogen bonding network to allow for facile transglycosyaltion, and stabilizing of the transition state. This is the first mechanism that utilizes experimental kinetics with theoretical calculations to propose a mechanism for metal catalyzed activation.

Lastly, experimental kinetics on magnesium's effect on activation to provide insight into the effect of ionic size are presented. Magnesium assisted activation exhibited identical behavior to the calcium case with energetics of activation matching within experimental error. Additional DFT calculations are required to determine if any changes of the mechanism occur due to a change in ion size.

A large amount of the metal catalyzed pyrolysis chemistry is still left to be discerned. Combining the PHASR technique with theoretical computations has demonstrated enormous potential to answer many of these questions. Further investigation into the role of other alkali and alkaline earth metals on activation should be conducted as well as their role in forming anyhydrosugars, light oxygenate and char.

Bibliography

1. Energy Information Administration, U. International Energy Outlook 2019 key takeaway. **2019**, (2020).
2. Chundawat, S. P. S., Beckham, G. T., Himmel, M. E. & Dale, B. E. Deconstruction of Lignocellulosic Biomass to Fuels and Chemicals. *Annu. Rev. Chem. Biomol. Eng.* **2**, 121–145 (2011).
3. Tan, Er. C. *et al. Process Design and Economics for the Conversion of Lignocellulosic Biomass to Hydrocarbons via Indirect Liquefaction*. *National Renewable Energy Laboratory: Pacific Northwest National Laboratory* (2015).
4. Shen, X., Kommalapati, R. & Huque, Z. The Comparative Life Cycle Assessment of Power Generation from Lignocellulosic Biomass. *Sustainability* **7**, 12974–12987 (2015).
5. European Commission. *Biofuels in the European Union A vision for 2030 and beyond*. *Final report of the Biofuels Research Advisory Council* (2006).
6. Huber, G. W., Iborra, S. & Corma, A. Synthesis of Transportation Fuels from Biomass. *Chem Rev.* **106**, 4044–4098 (2006).
7. Naik, S. N., Goud, V. V., Rout, P. K. & Dalai, A. K. Production of first and second generation biofuels : A comprehensive review. *Renew. Sustain. Energy Rev.* **14**, 578–597 (2010).
8. Himmel, M. E., Ding, S., Johnson, D. K. & Adney, W. S. Biomass Recalcitrance: Engineering Plants and Enzymes for Biofuels Production. *Science (80-.).* **315**, 804–808 (2007).
9. Stamm, A. Thermal Degradation of Wood and Cellulose. *Ind. Eng. Chem.* **48**, 413–417 (1956).
10. Bridgwater, A. V. Renewable fuels and chemicals by thermal processing of biomass. *Chem. Eng. J.* **91**, 87–102 (2003).
11. Mohan, D., Pittman, C. U. & Steele, P. H. Pyrolysis of Wood / Biomass for Bio-oil : A Critical Review. *Energy & Fuesl* **20**, 848–889 (2006).
12. Carlson, T. R., Vispute, T. P. & Huber, G. W. Green gasoline by catalytic fast pyrolysis of solid biomass derived compounds. *ChemSusChem* **1**, 397–400 (2008).
13. Furimsky, E. Catalytic hydrodeoxygenation. *Appl. Catal. A Gen.* **199**, 147–190 (2000).
14. De, S., Saha, B. & Luque, R. Hydrodeoxygenation processes: Advances

on catalytic transformations of biomass-derived platform chemicals into hydrocarbon fuels. *Bioresour. Technol.* **178**, 108–118 (2015).

15. Mettler, M. S., Vlachos, D. G. & Dauenhauer, P. J. Top ten fundamental challenges of biomass pyrolysis for biofuels. *Energy Environ. Sci.* **5**, 7797 (2012).

16. Hameed, S., Sharma, A., Pareek, V., Wu, H. & Yu, Y. A review on biomass pyrolysis models: Kinetic, network and mechanistic models. *Biomass and Bioenergy* **123**, 104–122 (2019).

17. Dauenhauer, P. J., Colby, J. L., Balonek, C. M., Suszynski, W. J. & Schmidt, L. D. Reactive boiling of cellulose for integrated catalysis through an intermediate liquid. *Green Chem.* **11**, 1555–1561 (2009).

18. Brennan Pecha, M., Montoya, J. I., Garcia-Perez, M., Chejne, F. & Ciesielski, P. N. Progress in understanding the four dominant intra-particle phenomena of lignocellulose pyrolysis: Chemical reactions, heat transfer, mass transfer, and phase change. *Green Chem.* **21**, 2868–2898 (2019).

19. Mettler, M. S. *et al.* Revealing pyrolysis chemistry for biofuels production: Conversion of cellulose to furans and small oxygenates. *Energy Environ. Sci.* **5**, 5414–5424 (2012).

20. Lynd, L. R., Wyman, C. E. & Gerngross, T. U. Biocommodity engineering. *Biotechnol. Prog.* **15**, 777–793 (1999).

21. Shahzadi, T. *et al.* Advances in lignocellulosic biotechnology: A brief review on lignocellulosic biomass and cellulases. *Adv. Biosci. Biotechnol.* **05**, 246–251 (2014).

22. Xu, C. & Ferdosian, F. Structure and Properties of Lignin. in *Conversion of Lignin into Bio-Based Chemicals and Materials* (2017).

23. El Khaldi-Hansen, B., Schulze, M. & Kamm, B. Qualitative and Quantitative Analysis of Lignins from Different Sources and Isolation Methods for an Application as a Biobased Chemical Resource and Polymeric Material. in *Analytical Techniques and Methods for Biomass* 15–45 (2016).

24. Agblevor, F. A. & Besler, S. Inorganic compounds in biomass feedstocks. 1. Effect on the quality of fast pyrolysis oils. *Energy & Fuels* **10**, 293–298 (1996).

25. Sorek, N., Yeats, T. H., Szemenyei, H., Youngs, H. & Somerville, C. R. The implications of lignocellulosic biomass chemical composition for the production of advanced biofuels. *Bioscience* **64**, 192–201 (2014).

26. Lédé, J. Cellulose pyrolysis kinetics: An historical review on the existence and role of intermediate active cellulose. *J. Anal. Appl. Pyrolysis* **94**, 17–32

(2012).

27. Demirbas, A. & Arin, G. An Overview of Biomass Pyrolysis. *Energy Sources* **24**, 471–482 (2002).

28. Katō, K. Pyrolysis of Cellulose. *Agric. Biol. Chem.* **31**, 657–663 (1967).

29. J. Lédé, J.P. Diebold, G:V.C Peacocke, J. P. The nature and properties of intermediate and unvaporized biomass pyrolisis materials. *Dev. Thermochem. biomass conversion.* 27–42 (1997).

30. Krumm, C. *et al.* Micro-Ratcheted Surfaces for a Heat Engine Biomass Conveyor. *Energy Environ. Sci.* **9**, 1645–1649 (2016).

31. Teixeira, A. R. *et al.* Reactive Liftoff of Crystalline Cellulose Particles. *Sci. Rep.* **5**, (2015).

32. Burnham, A. K., Zhou, X. & Broadbelt, L. J. Critical Review of the Global Chemical Kinetics of Cellulose Thermal Decomposition. *Energy & Fuels* **29**, 2906–2918 (2015).

33. Sánchez-Jiménez, P. E. *et al.* An improved model for the kinetic description of the thermal degradation of cellulose. *Cellulose* **18**, 1487–1498 (2011).

34. Sharma, A., Pareek, V. & Zhang, D. Biomass pyrolysis - A review of modelling, process parameters and catalytic studies. *Renew. Sustain. Energy Rev.* **50**, 1081–1096 (2015).

35. Mayes, H. B., Nolte, M. W., Beckham, G. T., Shanks, B. H. & Broadbelt, L. J. The alpha-bet(a) of glucose pyrolysis: Computational and experimental investigations of 5-hydroxymethylfurfural and levoglucosan formation reveal implications for cellulose pyrolysis. *ACS Sustain. Chem. Eng.* **2**, 1461–1473 (2014).

36. Laidler, K. J. *Chemical Kinetics*. (1987).

37. Wiberg, K. B. The Deuterium Isotope Effect. *Chem. Rev.* **55**, 713–743 (1955).

38. Westheimer, F. H. The magnitude of the primary kinetic isotope effect for compounds of hydrogen and deuterium. *Chem. Rev.* **61**, 265–273 (1961).

39. Hosoya, T. & Sakaki, S. Levoglucosan formation from crystalline cellulose: Importance of a hydrogen bonding network in the reaction. *ChemSusChem* **6**, 2356–2368 (2013).

40. Boutin, O., Ferrer, M. & Lédé, J. Radiant flash pyrolysis of cellulose—Evidence for the formation of short life time intermediate liquid species. *J. Anal. Appl. Pyrolysis* **47**, 13–31 (1998).

41. Bridgwater, A. V. Review of fast pyrolysis of biomass and product upgrading. *Biomass and Bioenergy* **38**, 68–94 (2012).

42. El-Sayed, S. A. & Mostafa, M. E. Pyrolysis characteristics and kinetic parameters determination of biomass fuel powders by differential thermal gravimetric analysis (TGA/DTG). *Energy Convers. Manag.* **85**, 165–172 (2014).

43. Xue, Y., Kelkar, A. & Bai, X. Catalytic co-pyrolysis of biomass and polyethylene in a tandem micropyrolyzer. *Fuel* **166**, 227–236 (2016).

44. Hoekstra, E., Van Swaaij, W. P. M., Kersten, S. R. A. & Hogendoorn, K. J. A. Fast pyrolysis in a novel wire-mesh reactor: Decomposition of pine wood and model compounds. *Chem. Eng. J.* **187**, 172–184 (2012).

45. Bradbury, A. G. W., Sakai, Y. & Shafizadeh, F. A Kinetic Model for Pyrolysis of Cellulose. *J Appl Polym Sci* **23**, 3271–3280 (1979).

46. Antal, M. J. & Varhegyi, G. Cellulose Pyrolysis Kinetics : The Current State of Knowledge. *Ind. Eng. Chem. Res.* **34**, 703–717 (1995).

47. Varhegyi, G., Jakab, E. & Antal, M. J. Is the Broido-Shafizadeh model for cellulose pyrolysis true? *Fuel Energy* **8**, 1345–1352 (1994).

48. Oasmaa, A. & Meier, D. Norms and standards for fast pyrolysis liquids: 1. Round robin test. *J. Anal. Appl. Pyrolysis* **73**, 323–334 (2005).

49. Maduskar, S., Facas, G. G., Papageorgiou, C., Williams, C. L. & Dauenhauer, P. J. Five Rules for Measuring Biomass Pyrolysis Rates: Pulse-Heated Analysis of Solid Reaction Kinetics of Lignocellulosic Biomass. *ACS Sustain. Chem. Eng.* **6**, 1387–1399 (2018).

50. Paulsen, A. D., Mettler, M. S. & Dauenhauer, P. J. The role of sample dimension and temperature in cellulose pyrolysis. *Energy and Fuels* **27**, 2126–2134 (2013).

51. Pakhomov, A. M. Free-radical mechanism of the thermodegradation of cellulose and formation of levoglucosan. *Russ. Chem. Bull.* **6**, 1525–1527 (1957).

52. Gardiner, D. The Pyrolysis of Some Hexoses and Derived Di-, Tri-, and Poly-saccharides. *J. Chem. Soc. C Org.* 1473–1476 (1966).

53. Mayes, H. B. & Broadbelt, L. J. Unraveling the Reactions that Unravel Cellulose. *J. Phys. Chem. A* **116**, 7098–7106 (2012).

54. Hwang, H., Oh, S., Cho, T. S., Choi, I. G. & Choi, J. W. Fast pyrolysis of potassium impregnated poplar wood and characterization of its influence on the formation as well as properties of pyrolytic products. *Bioresour.*

Technol. **150**, 359–366 (2013).

55. Patwardhan, P. R., Satrio, J. A., Brown, R. C. & Shanks, B. H. Influence of inorganic salts on the primary pyrolysis products of cellulose. *Bioresour. Technol.* **101**, 4646–4655 (2010).

56. Eom, I. Y. *et al.* Effect of essential inorganic metals on primary thermal degradation of lignocellulosic biomass. *Bioresour. Technol.* **104**, 687–694 (2012).

57. Müller-Hagedorn, M., Bockhorn, H., Krebs, L. & Müller, U. A comparative kinetic study on the pyrolysis of three different wood species. *J. Anal. Appl. Pyrolysis* **68**–**69**, 231–249 (2003).

58. Raveendran, K., Ganesh, A. & Khilar, K. C. Influence of mineral matter on biomass pyrolysis characteristics. *Fuel* **74**, 1812–1822 (1995).

59. Jung, Y. H. & Kim, K. H. Acidic Pretreatment. in *Pretreatment of Biomass: Processes and Technologies* 27–50 (2014). doi:10.1016/B978-0-12-800080-9.00003-7.

60. Maduskar, S. *et al.* Quantitative carbon detector (QCD) for calibration-free, high-resolution characterization of complex mixtures. *Lab Chip* **15**, 440–447 (2015).

61. Beach, C. A. *et al.* Quantitative carbon detector for enhanced detection of molecules in foods, pharmaceuticals, cosmetics, flavors, and fuels. *Analyst* **141**, 1627–1632 (2016).

62. Spanjers, C. S., Beach, C. A., Jones, A. J. & Dauenhauer, P. J. Increasing flame ionization detector (FID) sensitivity using post-column oxidation–methanation. *Anal. Methods* **9**, 1928–1934 (2017).

63. Krumm, C., Pfaendtner, J. & Dauenhauer, P. J. Millisecond Pulsed Films Unify the Mechanisms of Cellulose Fragmentation. *Chem. Mater.* **28**, 3108–3114 (2016).

64. Blasi, C. Di. Kinetic and Heat Transfer Control in the Slow and Flash Pyrolysis. *Ind. Eng. Chem. Res.* **35**, 37–46 (1996).

65. Lédé, J. Biomass Pyrolysis: Comments on Some Sources of Confusions in the Definitions of Temperatures and Heating Rates. *Energies* **3**, 886–898 (2010).

66. Ronsse, F., Dalluge, D., Prins, W. & Brown, R. C. Optimization of platinum filament micropyrolyzer for studying primary decomposition in cellulose pyrolysis. *J. Anal. Appl. Pyrolysis* **95**, 247–256 (2012).

67. Hamilton, L. H., Ayling, A. B. & Shibaoka, M. A new experimental device

for pyrolysing coal particles under controlled conditions over a wide range of heating rates. *Fuel* **58**, 873–876 (1978).

68. Zhu, C., Krumm, C., Facas, G. G., Neurock, M. & Dauenhauer, P. J. Energetics of cellulose and cyclodextrin glycosidic bond cleavage. *React. Chem. Eng.* **2**, 201–214 (2017).

69. Proano-Aviles, J., Lindstrom, J. K., Johnston, P. A. & Brown, R. C. Heat and Mass Transfer Effects in a Furnace-Based Micropyrolyzer. *Energy Technol.* **5**, 189–195 (2017).

70. Pecha, M. B., Montoya, J. I., Chejne, F. & Garcia-Perez, M. Effect of a Vacuum on the Fast Pyrolysis of Cellulose: Nature of Secondary Reactions in a Liquid Intermediate. *Ind. Eng. Chem. Res.* **56**, 4288–4301 (2017).

71. Ojha, D. K., Viju, D. & Vinu, R. Fast pyrolysis kinetics of alkali lignin: Evaluation of apparent rate parameters and product time evolution. *Bioresour. Technol.* **241**, 142–151 (2017).

72. Ltd., F. L. *Double-Shot Pyrolyzer PY-2020iD, Operation Manual*.

73. Alonso, D. M., Bond, J. Q. & Dumesic, J. a. Catalytic conversion of biomass to biofuels. *Green Chem.* **12**, 1493–1513 (2010).

74. SriBala, G., Carstensen, H. H., Van Geem, K. M. & Marin, G. B. Measuring biomass fast pyrolysis kinetics: State of the art. *Wiley Interdiscip. Rev. Energy Environ.* **8**, (2019).

75. Sekiguchi, Y. & Shafizadeh, F. The effect of inorganic additives on the formation, composition, and combustion of cellulosic char. *J. Appl. Polym. Sci.* **29**, 1267–1286 (1984).

76. Zhu, C., Maduskar, S., Paulsen, A. D. & Dauenhauer, P. J. Alkaline-Earth-Metal-Catalyzed Thin-Film Pyrolysis of Cellulose. *ChemCatChem* **8**, 818–829 (2016).

77. Carvalho, W. S., Cunha, I. F., Pereira, M. S. & Ataíde, C. H. Thermal decomposition profile and product selectivity of analytical pyrolysis of sweet sorghum bagasse: Effect of addition of inorganic salts. *Ind. Crops Prod.* **74**, 372–380 (2015).

78. Vinu, R. & Broadbelt, L. J. A mechanistic model of fast pyrolysis of glucose-based carbohydrates to predict bio-oil composition. *Energy Environ. Sci.* **5**, 9808–9826 (2012).

79. Lindstrom, J. K. *et al.* Competing reactions limit levoglucosan yield during fast pyrolysis of cellulose. *Green Chem.* **21**, 178–186 (2019).

80. Westmoreland, P. R. Pyrolysis kinetics for lignocellulosic biomass-to-oil

from molecular modeling. *Curr. Opin. Chem. Eng.* **23**, 123–129 (2019).

81. Seshadri, V. & Westmoreland, P. R. Roles of hydroxyls in the noncatalytic and catalyzed formation of levoglucosan from glucose. *Catal. Today* **269**, 110–121 (2016).

82. Maliekkal, V. *et al.* Activation of Cellulose via Cooperative Hydroxyl-Catalyzed Transglycosylation of Glycosidic Bonds. *ACS Catal.* **9**, 1943–1955 (2019).

83. Mettler, M. S., Paulsen, A. D., Vlachos, D. G. & Dauenhauer, P. J. The chain length effect in pyrolysis: bridging the gap between glucose and cellulose. *Green Chem.* **14**, 1284 (2012).

84. Trotta, F., Zanetti, M. & Camino, G. Thermal Degradation of Cyclodextrins. *Polym. Degrad. Stab.* 373–379 (2000).

85. Kresse, G. & Hafner, J. Ab initio molecular-dynamics simulation of the liquid-metalamorphous- semiconductor transition in germanium. *Phys. Rev. B* **49**, 14251–14269 (1994).

86. Kresse, G. & Hafner, J. Ab initio molecular dynamics for liquid metals. *Phys. Rev. B* **47**, 558–561 (1993).

87. Kresse, G. & Furthmüller, J. Efficient iterative schemes for ab initio total-energy calculations using a plane-wave basis set. *Phys. Rev. B - Condens. Matter Mater. Phys.* **54**, 11169–11186 (1996).

88. Perdew, J. P., Burke, K. & Ernzerhof, M. Generalized gradient approximation made simple. *Phys. Rev. Lett.* **77**, 3865–3868 (1996).

89. Grimme, S. Density functional theory with London dispersion corrections. *Wiley Interdiscip. Rev. Comput. Mol. Sci.* **1**, 211–228 (2011).

90. Grimme, S. Semiempirical GGA-Type Density Functional Constructed with a Long-Range Dispersion Correction. *J. Comput. Chem.* **27**, 1787–1799 (2006).

91. Kresse, G. & Joubert, D. From ultrasoft pseudopotentials to the projector augmented-wave method. *Phys. Rev. B - Condens. Matter Mater. Phys.* **59**, 1758–1775 (1999).

92. Pack, J. D. & Monkhorst, H. J. ‘special points for Brillouin-zone integrations’-a reply. *Phys. Rev. B* **16**, 1748–1749 (1977).

93. Henkelman, G., Uberuaga, B. P. & Jónsson, H. Climbing image nudged elastic band method for finding saddle points and minimum energy paths. *J. Chem. Phys.* **113**, 9901–9904 (2000).

94. Henkelman, G. & Jónsson, H. Improved tangent estimate in the nudged

elastic band method for finding minimum energy paths and saddle points. *J. Chem. Phys.* **113**, 9978–9985 (2000).

95. Henkelman, G. & Jónsson, H. A dimer method for finding saddle points on high dimensional potential surfaces using only first derivatives. *J. Chem. Phys.* **111**, 7010–7022 (1999).

96. Laue, W., Thiemann, M., Scheibler, E. & Wiegand, K. W. *Ullmann's Encyclopedia of Industrial Chemistry*. (Wiley-VCH, 2002).

97. Jensen, P. A., Frandsen, F. J., Dam-Johansen, K. & Sander, B. Experimental Investigation of the Transformation and Release to Gas Phase of Potassium and Chlorine during Straw Pyrolysis. *Energy & Fuels* **14**, 1280–1285 (2000).

98. Center, N. M. S. D. & Wallace, W. E. Mass Spectra. in *NIST Chemistry WebBook*.

99. Friedel, R. A., Shultz, J. L. & Sharkey, A. G. Mass Spectrum of Nitric Acid. *Anal. Chem.* **31**, 1128 (1959).

100. Mayes, H. B. *et al.* Sodium ion interactions with aqueous glucose: Insights from quantum mechanics, molecular dynamics, and experiment. *J. Phys. Chem. B* **118**, 1990–2000 (2014).

101. Arora, J. S., Chew, J. W. & Mushrif, S. H. Influence of Alkali and Alkaline-Earth Metals on the Cleavage of Glycosidic Bond in Biomass Pyrolysis: A DFT Study Using Cellobiose as a Model Compound. *J. Phys. Chem. A* **122**, 7646–7658 (2018).

102. Saddawi, A., Jones, J. M. & Williams, A. Influence of alkali metals on the kinetics of the thermal decomposition of biomass. *Fuel Process. Technol.* **104**, 189–197 (2012).

103. Bugg, C. E. Calcium Binding to Carbohydrates. Crystal Structure of a Hydrated Calcium Bromide Complex of Lactose. *J. Am. Chem. Soc.* **95**, 908–913 (1973).

104. Cook, W. J. & Bugg, C. E. Calcium Binding to Galactose. Crystal Structure of a Hydrated -Galactose---Calcium Bromide Complex. *J. Am. Chem. Soc.* **95**, 6442–6446 (1973).

105. Hosoya, T., Nakao, Y., Sato, H., Kawamoto, H. & Sakaki, S. Thermal degradation of methyl β-D-glucoside. A theoretical study of plausible reaction mechanisms. *J. Org. Chem.* **74**, 6891–6894 (2009).

106. Seshadri, V. & Westmoreland, P. R. Concerted reactions and mechanism of glucose pyrolysis and implications for cellulose kinetics. *J. Phys. Chem. A* **116**, 11997–12013 (2012).

107. Rodriguez Quiroz, N., Norton, A. M., Nguyen, H., Vasileiadou, E. & Vlachos, D. G. Homogeneous metal salt solutions for biomass upgrading and other select organic reactions. *ACS Catal.* **9**, 9923–9952 (2019).

108. Saijonkari-Pahkala, K. Non-wood plants as raw material for pulp and paper. *Agric. Food Sci. Finl.* **10**, 10–95 (2001).

109. Plumley, J. A. & Evanseck, J. D. Periodic trends and index of boron lewis acidity. *J. Phys. Chem. A* **113**, 5985–5992 (2009).

110. Shannon, R. D. Revised Effective Ionic Radii and Systematic Studies of Interatomie Distances in Halides and Chaleogenides BY. *Acta Crystallogr. Sect. A* **32**, 751–767 (1976).

111. Lock, R. H., Lock, P. F., Lock Morgan, K., Lock, E. F. & Lock, D. F. *Statistics: Unlocking the Power of Data*. (2013).

112. Nishiyama, Y., Langan, P. & Chanzy, H. Crystal structure and hydrogen-bonding system in cellulose Iβ from synchrotron X-ray and neutron fiber diffraction. *J. Am. Chem. Soc.* **124**, 9074–9082 (2002).